SPi	Journal Code				Article ID					Dispatch: 27.02.19	CE: RJS
	G	B	C		2	0	8	5	2	No. of Pages: 27	ME:

Global Biogeochemical Cycles

RESEARCH ARTICLE
10.1029/2018GB005975

Key Points:
- Dissolved Zn profiles in the Western Arctic do not have the typical "nutrient-type" profile shape found in the Atlantic and Pacific Oceans
- Arctic Zn is controlled by shelf fluxes from porewater remineralization of Zn-rich phytoplankton and water mass mixing of preformed Zn
- Arctic Zn:Si slope is higher than the global mean and weakly correlated, due to shelf Zn enrichment and decoupling of Zn:Si in deep waters

Supporting Information:
- Supporting Information S1
- Data Set S1

Correspondence to:
J. N. Fitzsimmons,
jessfitz@tamu.edu

Citation:
Jensen, L. T., Wyatt, N. J., Twining, B. S., Rauschenberg, S., Landing, W. M., Sherrell, R. M., & Fitzsimmons, J. N. (2019). Biogeochemical cycling of dissolved zinc in the Western Arctic (Arctic GEOTRACES GN01). *Global Biogeochemical Cycles*, *33*. https://doi.org/10.1029/2018GB005975

Received 2 MAY 2018
Accepted 2 FEB 2019
Accepted article online 15 FEB 2019

Biogeochemical Cycling of Dissolved Zinc in the Western Arctic (Arctic GEOTRACES GN01)

L. T. Jensen[1], N. J. Wyatt[2,3], B. S. Twining[4], S. Rauschenberg[4], W. M. Landing[2], R. M. Sherrell[5,6], and J. N. Fitzsimmons[1]

[1]Department of Oceanography, Texas A&M University, College Station, TX, USA, [2]Department of Earth, Ocean and Atmospheric Science, Florida State University, Tallahassee, FL, USA, [3]School of Ocean and Earth Sciences, National Oceanography Centre, University of Southampton, Southampton, UK, [4]Bigelow Laboratory for Ocean Sciences, Boothbay, ME, USA, [5]Department of Marine and Coastal Sciences, Rutgers University, New Brunswick, NJ, USA, [6]Department of Earth and Planetary Sciences, Rutgers University, Piscataway, NJ, USA

Abstract The biogeochemical cycling of dissolved zinc (dZn) was investigated in the Western Arctic along the U.S. GEOTRACES GN01 section. Vertical profiles of dZn in the Arctic are strikingly different than the classic "nutrient-type" profile commonly seen in the Atlantic and Pacific Oceans, instead exhibiting higher surface concentrations (~1.1 nmol/kg), a shallow subsurface absolute maximum (~4–6 nmol/kg) at 200 m coincident with a macronutrient maximum, and low deep water concentrations (~1.3 nmol/kg) that are homogenous with depth. In contrast to other ocean basins, typical inputs such as rivers, atmospheric inputs, and especially deep remineralization are insignificant in the Arctic. Instead, we demonstrate that dZn distributions in the Arctic are controlled primarily by (1) shelf fluxes following the sediment remineralization of high Zn:C and Zn:Si cells and the seaward advection of those fluxes and (2) mixing of dZn from source waters such as the Atlantic and Pacific Oceans rather than vertical biological regeneration of dZn. This results in both the unique profile shapes and the largely decoupled relationship between dZn and Si found in the Arctic. We found a weak dZn:Si regression in the full water column (0.077 nmol/μmol, $r^2 = 0.58$) that is higher than the global slope (0.059 nmol/μmol, $r^2 = 0.94$) because of the shelf-derived halocline dZn enrichments. We hypothesize that the decoupling of Zn:Si in Western Arctic deep waters results primarily from a past ventilation event with unique preformed Zn:Si stoichiometries.

Plain Language Summary The Arctic Ocean is a highly understudied ocean basin that is experiencing rapid changes as a result of climate change that are already affecting the Arctic ecosystem. Understanding nutrient sources and sinks in the Arctic is critical to predicting how the nutrient supply to Arctic organisms might change upon future climate change. Zinc is a micronutrient that, while not limiting to most photosynthesizing ocean plankton, does play a role in the community composition of these plankton. We measured dissolved zinc distributions in the Western Arctic Ocean for the first time and found them to be strikingly different from the classic "nutrient-type" profile of other ocean basins. Only over the shallow continental margin did biological zinc cycling dominate its distribution; otherwise, zinc was determined mostly by mixing between Atlantic and Pacific incoming waters, without biological overprinting. Additionally, the largest zinc source was from the regeneration of zinc-rich cells in sediment porewaters over the Chukchi shelf, and this zinc was transported far offshore in the Arctic halocline. Surprisingly, typical zinc sources such as rivers, atmospheric inputs, and especially deep regeneration were insignificant in the Arctic.

1. Introduction

Zinc (Zn) is an essential physiological nutrient for marine microorganisms, supporting carbon and organic phosphorus acquisition, protein structure, and DNA replication (Morel, 2008). The availability of Zn has been shown to regulate microbial activity in laboratory culture experiments (Cox & Saito, 2013; Shaked et al., 2006; Sunda & Huntsman, 1995) and, more recently, in natural ocean systems (Crawford et al., 2003; Franck et al., 2003; Jakuba et al., 2012; Mahaffey et al., 2014). This has increased awareness of the important role for Zn in oceanic primary production and carbon export. While the extent to which surface dissolved Zn (dZn) concentrations limit oceanic primary production remains unclear, investigations of the processes that mediate Zn's surface water inputs and removal fluxes, deep water regeneration, and surface

resupply are at the forefront of modern trace metal biogeochemistry (Boyd et al., 2017; Little et al., 2016, 2014; Vance et al., 2017; Wyatt et al., 2014).

Globally, the vertical oceanic distribution of dZn resembles that of the macronutrients, with surface depletion resulting from biological uptake and high concentrations at depth from regeneration (Schlitzer et al., 2018). In most oceanic surface waters, dZn concentrations are typically <0.2 nmol/kg (Conway & John, 2014; Gosnell et al., 2012; Lohan et al., 2002; Wyatt et al., 2014), and dZn is strongly complexed (>95%) by organic ligands (Bruland, 1989; Ellwood & van den Berg, 2000; Jakuba et al., 2012). In the deep ocean, dZn concentrations increase from 2 nmol/kg in the North Atlantic (Conway & John, 2014) to around 10 nmol/kg in the North Pacific (Bruland, 1980; Bruland & Lohan, 2003) as water masses age and accumulate Zn from regenerated material. However, this simplistic uptake and regeneration-based paradigm for oceanic Zn cycling is often insufficient to explain observational data, where a complex array of physical and biogeochemical interactions, including external inputs and horizontal mixing (Kondo et al., 2016; Roshan & Wu, 2015; Vance et al., 2017), scavenging onto organic matter (John & Conway, 2014), and authigenic Zn sulfide precipitation (Conway & John, 2015; Janssen & Cullen, 2015) may also be important.

Riverine inputs are widely regarded as the dominant source of dZn to the oceans, based on a global riverine Zn flux of 5.9×10^8 mol/year that is an order of magnitude higher than the atmospheric flux (Little et al., 2014). There is also evidence for a hydrothermal source of Zn (Conway & John, 2014; Roshan & Wu, 2015; Roshan et al., 2016), although the significance of this flux to the global ocean dZn inventory remains uncertain because of the paucity of far-field hydrothermal measurements. The principle removal mechanism for Zn from the oceanic inventory is the burial of organic and authigenic material in seafloor sediments (Little et al., 2016, 2014). The large sedimentary Zn inventory (Cai et al., 2011; Trefry et al., 2014) may act as a source of Zn to the water column under certain conditions (Conway & John, 2015; Kondo et al., 2016).

Zn also exhibits a remarkably tight correlation with dissolved silicate (Si) in the Atlantic, Pacific, and Southern Oceans, showing a deeper remineralization depth than nitrate (N) and phosphate (P; Schlitzer et al., 2018). This would imply that the oceanic cycle of Zn is dominated by uptake into and regeneration from diatom siliceous tests, which are regenerated more slowly during sinking through the water column than intracellular organic matter (Zhao et al., 2014). However, the vast majority of Zn in diatoms is associated with N and P in organic tissues (Twining & Baines, 2013; Twining et al., 2004, 2015) and not diatom opal (1–3% of total cellular Zn inventory; Ellwood & Hunter, 2000; Jaccard et al., 2009), and thus, Zn should be regenerated from this organic matter in the upper ocean alongside P rather than opal-derived Si (Twining et al., 2014). A more recent hypothesis suggests that the strong Zn-Si correlation across the major oceans is instead explained by extreme drawdown of Zn and Si relative to P by diatoms in the surface Southern Ocean, and it is the lateral transport and modification of these Zn- and Si-depleted waters that sets the unusual Zn-Si-P stoichiometry in global nutricline waters (Ellwood, 2008; Vance et al., 2017; Weber et al., 2018; Wyatt et al., 2014). Many of our global conclusions on Zn biogeochemistry have come from studies in low and middle latitudes, with relatively little work done in the polar oceans (Cid et al., 2012; Kondo et al., 2016). Given the interconnections between the polar and lower-latitude oceans through deep and intermediate water formation and circulation, knowledge of polar ocean Zn biogeochemistry is critical to understanding its potential impact on Zn distributions across the global ocean.

Here we investigate the dominant biogeochemical processes controlling the Zn distribution in the Arctic Ocean, where until very recently only four profiles of Zn had been published decades ago (Danielsson & Westerlund, 1983; Moore, 1981; Yeats, 1988; Yeats & Westerlund, 1991). The Arctic Ocean is a small, enclosed basin accounting for ~3% of the global ocean by area (Chang & Devol, 2009), where circulation is driven by a unique bottom bathymetry. Approximately 50% of its surface area overlies continental shelves (Jakobsson et al., 2004) such that margin processes play a much greater role in regulating trace metal distributions than in other major oceans (Cid et al., 2012; Kondo et al., 2016). The Arctic communicates with the North Atlantic Ocean through the deep Fram Strait and also receives inputs from the North Pacific through the shallow and narrow Bering Strait. A common tracer of Pacific waters in the Arctic is elevated Si concentration (Jones & Anderson, 1986), and since Si and Zn are well correlated in the global ocean, we hypothesized that Zn might also be a Pacific water tracer. Cid et al. (2012) and Kondo et al. (2016) recently identified a dZn concentration maximum associated with the macronutrient maximum of the upper halocline, suggesting that dZn distributions are generally controlled by the same biological cycles influencing the

macronutrients compared to the shelf-based sources and/or removal processes suggested for iron (Aguilar-Islas et al., 2013; Cid et al., 2012; Hioki et al., 2014; Kondo et al., 2016). However, the mechanism for the transport of Zn from the shelves into the interior Arctic Ocean remains unclear.

We report the full water column distribution of dZn for the Western Arctic Ocean during late summer 2015 sampled along the U.S. GEOTRACES GN01 section. In contrast to other ocean basins, Zn sources such as atmospheric inputs and especially deep remineralization are less significant in the open Arctic. We show that mixing between North Pacific and North Atlantic source waters, as well as the influence of shelf sediment remineralization sources, dominates dZn biogeochemistry. These measurements are timely, given ongoing climate change in the Arctic, as they provide a baseline for interpreting observations of Arctic biogeochemistry upon future environmental change.

2. Methods

2.1. Sample Collection

Seawater samples were collected during the 2015 U.S. Arctic GEOTRACES (GN01) cruise aboard the USCGC Healy (HLY1502), which departed from Dutch Harbor, AK, on 9 August 2015 and returned 12 October 2015. The cruise track (Figure 1) began in the North Pacific (~60°N, Station 1), traversed the Bering Shelf (Stations 2 and 3) and through the Bering Strait (Stations 4 and 5), across the Chukchi Shelf (Stations 6–8), and northward along ~170°W ("northbound," Stations 10–30) to the North Pole (Station 32). The cruise track then returned south along 150°W ("southbound," Stations 33–57) and ended on the Chukchi Shelf (Stations 61–66). There was increased sampling resolution along the shelf-break (Stations 8–14 and 57–66) for a total of 23 full-depth trace metal stations, 4 shallow-depth ice hole stations (Stations 31, 33, 39, and 43), and 4 middepth marginal ice zone stations (Stations 8, 51, 53, and 54). F1

Seawater sample collection followed established GEOTRACES sampling protocols (Cutter et al., 2010). Briefly, seawater was collected using a trace-metal clean Seabird carousel/CTD with a Vectran cable and 24 × 12-L Go-Flo bottles. Two bottles were tripped per depth on ascent at ~3 m/min. Upon recovery, each Go-Flo was pressurized to ~0.5 atm. with HEPA-filtered air and fitted with a 0.2-μm AcroPak-200 polyethersulfone membrane filter capsule (Pall), and seawater was filtered into 250-ml LDPE Nalgene bottles following three 10% volume rinses of the bottle, cap, and threads. Bottles were cleaned prior to sampling using established protocols with hydrochloric acid (trace metal grade HCl, 1 M) and ultrapure Milli-Q water at 60 °C (Fitzsimmons & Boyle, 2012). Samples were acidified to pH 1.8 (flow injection analysis [FIA], 0.024 M using quartz-distilled HCl) and 2.0 (inductively coupled plasma mass spectrometer [ICP-MS], 0.012 M using Optima, Fisher Scientific) and stored at room temperature. Q5

Near-surface seawater samples were collected through holes in sea ice floes (Stations 31, 33, 39, and 43) at 1, 5, and 20 m using a polypropylene high-head battery-powered enclosed motor centrifugal pump with 0.5-in. FEP-lined Tygon tubing (Cole Parmer). Samples were collected and filtered (0.2 μm, AcroPak) on the ice into a 25-L acid-cleaned carboy and were subsampled into clean 250-ml LDPE Nalgene bottles, acidified, and stored as above. Q6

2.2. Zn Analysis and Intercomparison

2.2.1. FIA

Dissolved Zn analysis was performed onboard ship using FIA with fluorimetric detection, under a HEPA filter unit within a shipboard purpose-built clean environment. The FIA system was a modified version of the system described in Nowicki et al. (1994) and more recently in Wyatt et al. (2014) using the fluorescent binding ligand p-tosyl-8-aminoquinoline (pTAQ). Briefly, the sample was buffered inline to pH 5.0 using 0.3-M ammonium acetate (Optima, Fisher Scientific), yielding a final concentration of 0.12-M ammonium acetate in the samples, before Zn (II) was selectively preconcentrated for 1 min onto the cation exchange resin Toyopearl AF-Chelate 650M. Interfering seawater constituents were removed from the resin by rinsing for 30 s with 0.08-M ammonium acetate before the Zn (II) was liberated from the resin using 0.08-M quartz-distilled HCl. The eluent was mixed with a 50-μM pTAQ (Sigma-Aldrich) solution, and the fluorescent emission of the Zn-pTAQ complex was detected using a Shimadzu RF-10Axl fluorimeter with excitation and emission wavelengths set to 377 and 495 nm, respectively.

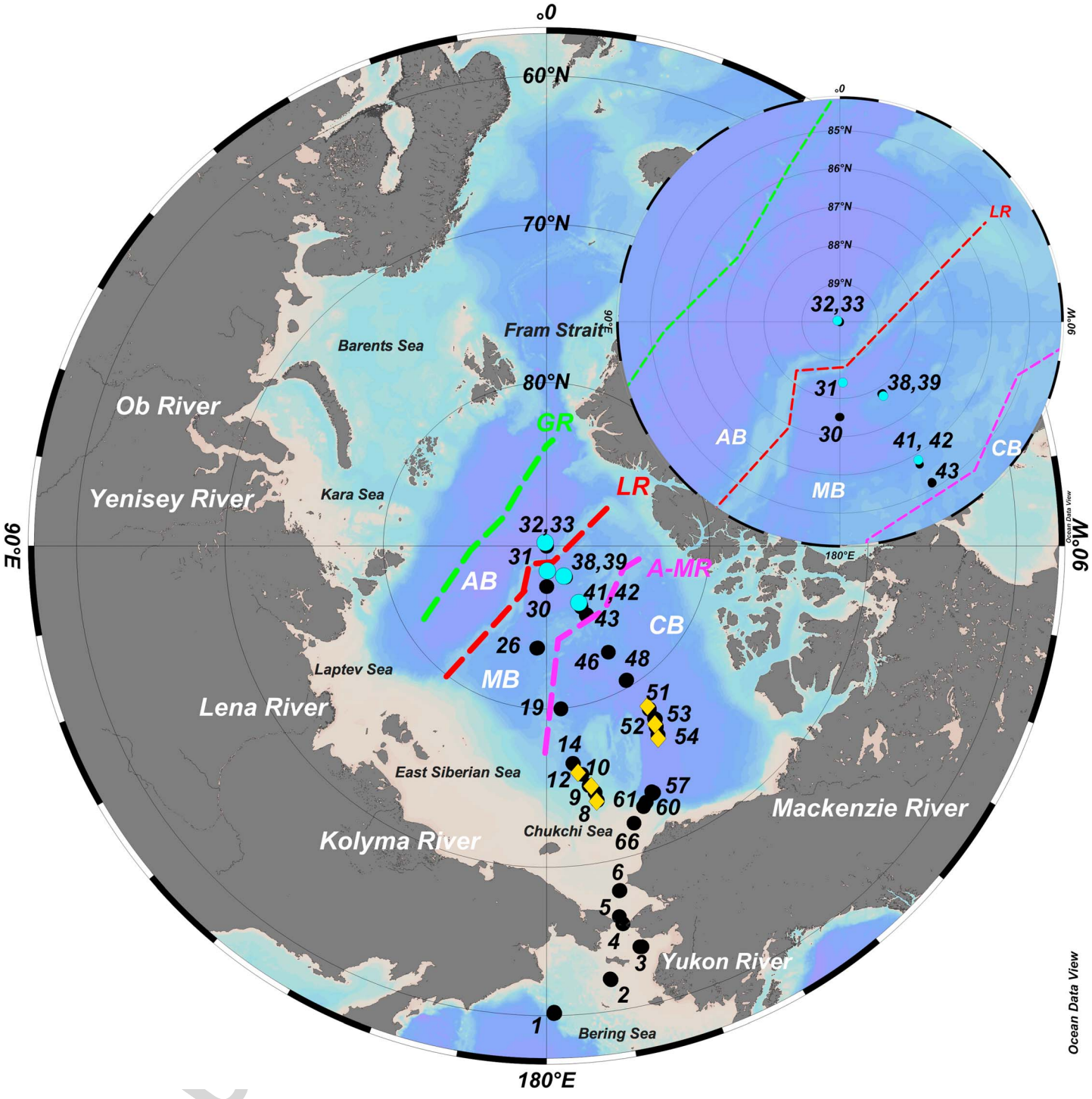

Figure 1. U.S. GEOTRACES Arctic GN01 transect with relevant stations, rivers, seas, and bathymetric features identified. Blue dots = ice Stations 31, 33, 39, and 42; orange diamonds = MIZ Stations 8, 9, 10, 12, 52, 53, and 54; black dots = full-depth stations. AB = Amundsen Basin, MB = Makarov Basin, CB = Canada Basin, GR = Gakkel Ridge, LR = Lomonosov Ridge, A-MR = Alpha-Mendeleev Ridge. Station 1 is used as a North Pacific end member analog. Stations 1–3 are considered "Bering Shelf." Stations 4 and 5 are considered "Bering Strait." Stations (6–9, 61–66) are considered "Chukchi Shelf." Stations 10–31 are "northbound" transect, Station 32 is the North Pole, and Stations 38–60 are "southbound" transect. Inset shows detail to differentiate ice stations from full-depth stations.

Zinc standards (0–8 nmol/kg) were prepared in 0.2-μm-filtered, low-Zn surface seawater. The analytical blank, determined by loading acidified (0.024 M quartz-distilled HCl, pH 1.7) ultrapure water treated as a sample, was typically <0.15 nmol/kg. The limit of detection (3 × σ of the lowest standard addition) was

Table 1
Measured Values for GEOTRACES Reference Materials SAFe D1 and D2 Across Three Labs and Two Analytical Methods

Reference material	Measured value	Consensus value (May 2013)
SAFe D1 (SeaFAST TAMU)	7.37 (±0.27) nmol/kg, $n = 43$	7.40 (±0.35) nmol/kg
SAFe D1 (SeaFAST Rutgers)	7.32 (±0.15) nmol/kg, $n = 4$	
SAFE D2 (SeaFAST TAMU)	7.36 (±0.23) nmol/kg, $n = 43$	7.43 (±0.25) nmol/kg
SAFe D2 (FIA FSU)	7.30 (±0.23) nmol/kg, $n = 10$	

Note. FIA = flow injection analysis; FSU = Florida State University; TAMU = Texas A&M University.

<0.05 nmol/kg for a 1-min load time, while the relative standard deviation (RSD) for replicate analyses was 0–5%. The accuracy of the analytical method was validated by quantification of dZn in the SAFe D2 reference sample (Table 1, "FIA"). T1

Cadmium is also known to form a fluorescent complex with the reagent pTAQ. The Cd interference for the method was investigated by spiking low-Zn seawater with single and combination additions of Zn and Cd (1–10 nmol/kg from 1,000 ppm Zn (II) and Cd (II) ICP-MS standards). The Cd interference from this standard matrix was estimated to be equivalent to ~4.5% of the analytical signal. This interference was corrected using the Cd concentration for each sample, measured using a ^{111}Cd isotope spike at Texas A&M University (TAMU) simultaneously with Zn, as described below in section 2.2.2.

2.2.2. SeaFAST/ICP-MS

At least 9 months after acidification, samples were analyzed for their Zn concentration at TAMU using isotope dilution and Zn preconcentration on a SeaFAST-pico system (ESI, Omaha, NE) following a modified, offline version of Lagerström et al. (2013). An acidified seawater sample (10 ml) was weighed and then spiked with ^{68}Zn and loaded into the SeaFAST autosampler, which automates mixing with a 5.90 N ammonium acetate buffer (Optima, Fisher Scientific) to adjust to an optimal pH around 6.5 (Sohrin et al., 2008). The buffered sample-spike mixture was then loaded onto a 200-µl column filled with Nobias-chelate PA1 resin, followed by rinsing with ultrapure water to remove salts. The Zn collected on the column was then eluted using 1.6-M HNO_3 (Optima, Fisher Scientific). Rather than online elution directly into the ICP-MS, 400 µl of eluent was captured (for a 25-fold preconcentration) in acid-cleaned 1.5-ml centrifuge tubes (Micrewtube®) and stored up to 1 week before analysis. Elemental analysis was accomplished in medium resolution on a Thermo Finnigan Element XR high-resolution ICP-MS (HR-ICP-MS) housed at the R. Ken Williams Radiogenic Isotope Facility. At least 20 procedural blanks composed of acidified (0.012-M HCl Optima, Fisher Scientific), ultrapure Milli-Q water (Element-POD, Millipore) for every 40 seawater samples were run through the spike, preconcentration, and analysis sequence to evaluate the contribution of dZn from reagents and the SeaFAST system. Blanks for dZn averaged 0.18 nmol/kg and generally decreased over time with increased SeaFAST system usage, becoming as low as 0.050 nmol/kg in the later analytical sessions. The detection limit of this method, taken as $3 \times \sigma$ of the procedural blanks, averaged 0.07 nmol/kg over all runs. The accuracy of the analytical method was validated by quantification of dZn in the SAFe D1 and D2 reference samples (Table 1, "SeaFAST (TAMU)"). Precision was evaluated over replicate analyses ($n = 96$) of random samples within the data set, yielding an RSD of 0–6%, compared to 3% precision in the SAFe D1 and D2 standards.

2.2.3. Intercomparison of Subsampling and Analytical Techniques

An intercomparison of dZn concentrations between TAMU, Florida State University (FSU), and Rutgers University was performed in order to assess the reliability and accuracy of the FIA and SeaFAST methods (Figure 2). Unique seawater samples from Station 19 were collected by both FSU and TAMU teams on F2 the Arctic cruise, and subsequently aliquots from TAMU were sent to Rutgers for evaluation by their methods. Analytically, FSU performed the FIA dZn analysis, while both TAMU and Rutgers employed the SeaFAST-pico isotope dilution technique, with analysis on different HR-ICP-MS instruments (for Rutgers on a Finnigan MAT Element 1 HR-ICP-MS, procedural blank = 0.06 nmol/kg). In general, the data generated by the three different laboratories agree well, with an average RSD of 6%, except at depths 450 and 500 m. This RSD agreed well with the reported precision for each method, as stated above.

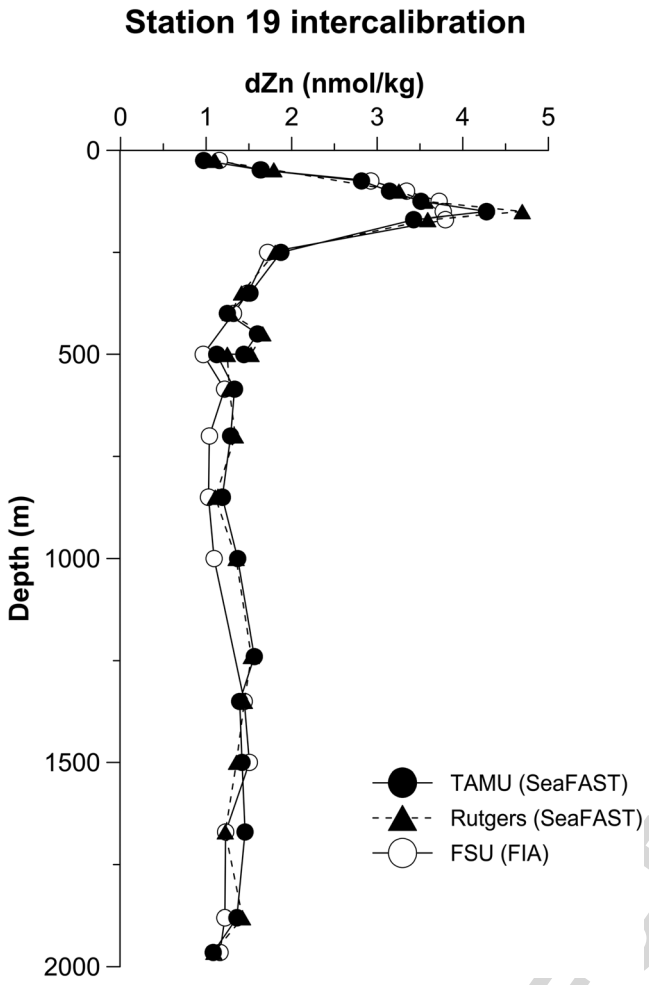

Figure 2. Full-depth intercalibration between two SeaFAST pico isotope dilution methods from TAMU (filled circles) and Rutgers (filled triangles), and FIA fluorometric methods at FSU (open circles). The results from Station 19 showed an average relative standard deviation of 6% across the three labs. FIA; FSU = Florida State University; TAMU = Texas A&M University.

2.3. Temperature, Salinity, Nutrients, and Hydrography

Temperature and pressure were determined by the trace metal CTD sensors (Seabird 911+). Bottle salinity was measured on unfiltered subsamples using a shipboard Guildline Autosal 8400B salinometer at room temperature, while dissolved oxygen analyses were performed using a modified Winkler titration (Carpenter, 1965; Culberson et al., 1991) with water taken from a separate cast and CTD operated by the Scripps Institution of Oceanography (SIO). Dissolved macronutrients nitrate, nitrite, phosphate, and silicate were analyzed shipboard at room temperature on a Seal Analytical continuous-flow AutoAnalyzer 3 following the methods described in the GO-SHIP repeat hydrography manual (Hydes et al., 2010). All isosurface and contoured sections in this paper were prepared using the Ocean Data View software (Schlitzer, 2016).

2.4. SXRF Cell Stoichiometry Analyses

Single-cell synchrotron X-ray fluorescence (SXRF) samples were collected from the surface mixed layer using the GEOTRACES rosette. Unfiltered water samples were preserved with 0.25% trace-metal clean buffered glutaraldehyde (Twining et al., 2003) and centrifuged onto 1 × 1-mm, 200-μm-thick SiN windows. Windows were briefly rinsed with a drop of ultrapure water and dried in a Class-100 cabinet. SXRF analysis was performed using the 2-ID-E beamline at the Advanced Photon source (Argonne National Laboratory) following the protocols of Twining et al. (2011). Each cell was raster scanned with a focused 10-keV X-ray beam with a diameter of approximately 0.5 μm. Fluorescence spectra from the pixels covering the cell were averaged to calculate whole-cell quotas, and a fluorescence spectrum from a neighboring empty section of the grid was subtracted. Cellular Zn and Si_{α} fluorescence intensities were fit with a modified-Gaussian model using custom software and peak areas converted to areal element concentrations using NBS-certified standard reference materials (Núnez-Milland et al., 2010; Twining et al., 2011). Spatial regions of interest representing the whole cell (including any adsorbed elements, if present) were prepared for each cell and used to calculate Zn and Si quotas. Cellular C quotas were calculated from cell biovolume using the equations of Menden-Deuer and Lessard (2000). Cell biovolume was calculated for each cell from measurements of cell diameter, length, and height using digital image processing software Image J. Shape and volume equations were taken from Hillebrand et al. (1999). In total, 119 cells were analyzed, with 13–24 cells analyzed at each station.

3. Results and Discussion

Dissolved Zn concentrations in seawater across the entire U.S. Arctic GEOTRACES GN01 section ranged 0.37–6.59 nmol/kg, averaging 1.77 ± 0.96 overall (n = 321). As can be seen in Figure 3, a characteristic dZn depth profile in the Western Arctic (representative Station 52) has a very different shape from those in the other major ocean basins. Instead of the classic nutrient-type profile shape of the Atlantic and Pacific, with ≤0.2-nmol/kg concentrations in the surface that increase to maximum values at depth, the Western Arctic dZn concentrations were elevated even at the surface, climbed to a maximum near 250-m depth and had lowest concentrations below 2,000-m depth (Figure 3b). Here we explain this unique profile shape as a result of water mass mixing, external dZn fluxes, and internal biological cycling alongside the macronutrient Si. We then return to a comparison to global dZn distributions.

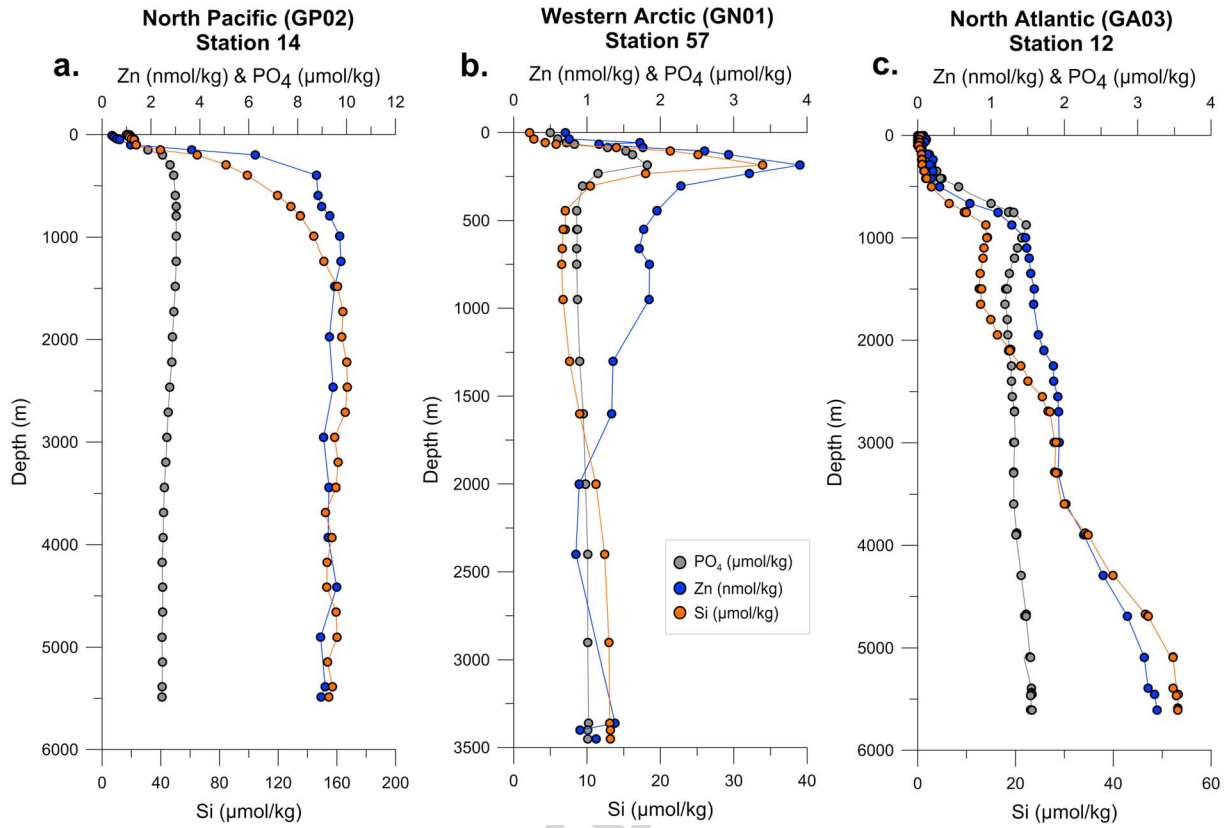

Figure 3. Global comparison of P, Si, and dZn profiles in the (a) North Pacific GP02 (Station 14,47.0°N/170.0°W), (b) Western Arctic GN01 (Station 57, this study,73.4°N/156.5°W), and (c) North Atlantic GA03 (Station 12, 29.7°N/56.8°W; Schlitzer et al., 2018). Dissolved zinc has a uniquely different profile shape in the Arctic compared to the classic nutrient-type profiles characteristic of other ocean basins.

3.1. Hydrographic Setting

The Arctic Ocean is a semienclosed basin with several bathymetrically defined subbasins. The Western Arctic, also known as the Amerasian Basin, is delineated west of the Lomonosov Ridge and contains the Canada and Makarov subbasins, which are separated by the Alpha and Mendeleev Ridges (Figure 1). Station 32 of this study, located at the geographic North Pole, is the only station from GN01 located east of the Lomonosov Ridge in the Amundsen Basin, which is part of the greater Eurasian Basin.

The water masses of the Western Arctic Ocean along GN01 are defined by their thermohaline and macronutrient properties (Figure 4). Arctic surface waters, often referred to as the Polar Mixed Layer (PML; Rudels, 2015), in the Western Arctic originate primarily from Pacific water that is advected through the shallow Bering Strait (50-m sill). The fresh, nutrient-rich PML extends variably from ~0–50 m and has salinity (S) ranging from 22 to 31 and potential temperature (θ) of −1.8 to 1.8 °C. Here we define the surface PML (sPML) as 0–25 m in order to differentiate it from the deeper PML that may mix with underlying waters. F4

The deep edge of the PML is delineated by a sharp increase in salinity, leading into the water mass known as the halocline. The halocline is generated during sea ice formation from PML waters on the Arctic shelves, creating a salty, cold water mass that subducts below the fresher PML (Aagaard, 1981; Jones & Anderson, 1986). A striking feature of the Western Arctic is the diversity of halocline structures present in the Canada and Makarov Basins (Figures 4 and 5) described below (Bluhm et al., 2015). F5

The Makarov Basin has a single halocline (θ −1.5–0.7 °C, S 31–34.3), primarily derived from Eurasian shelf waters and mixing from the Atlantic layer below (Rudels, 2015). Similarly, the Amundsen Basin (Station 32) has a broad, single halocline (θ −1.8–1.6 °C, S 32.7–34.7) and is also formed from the Eurasian shelves (Rudels et al., 2004). In contrast, the Canada Basin has a “double halocline” (Figures 4a, 5a, and 5c), separated by a halostad, where the upper halocline layer (UHL: θ −1.5– 0.4 °C, S 31–33.1) is formed primarily

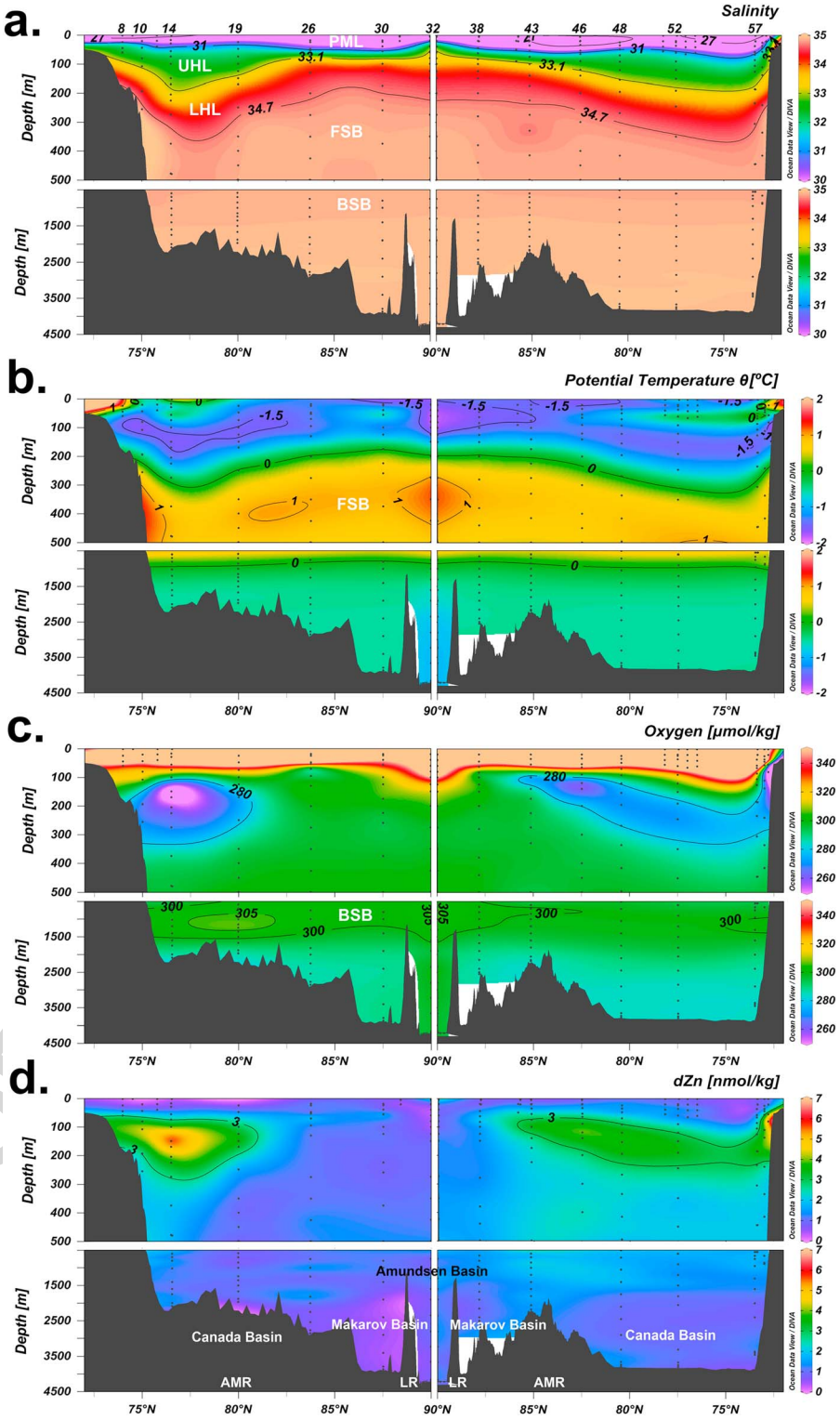

Figure 4. Water mass characteristics for the northbound (left) and southbound (right) transects in the upper 500 m (top) and >500 m (bottom). (a) Salinity with contours to differentiate major water masses: Polar Mixed Layer (PML), upper halocline layer (UHL), lower halocline layer (LHL), Fram Strait branch (FSB), and Barents Sea branch (BSB) of the Atlantic layer. b) Potential temperature with contours highlighting the temperature maximum indicative of the FSB. (c) Oxygen with contours showing the UHL oxygen minimum and the BSB maximum. (d) Dissolved zinc with a contour of 3 nmol/kg to highlight the concentration maximum within the UHL. Labels in (d) delineate the basin boundaries for the Makarov, Canada, and Amundsen Basins, as well as the Lomonosov Ridge (LR) and Alpha-Mendeleev Ridge (AMR).

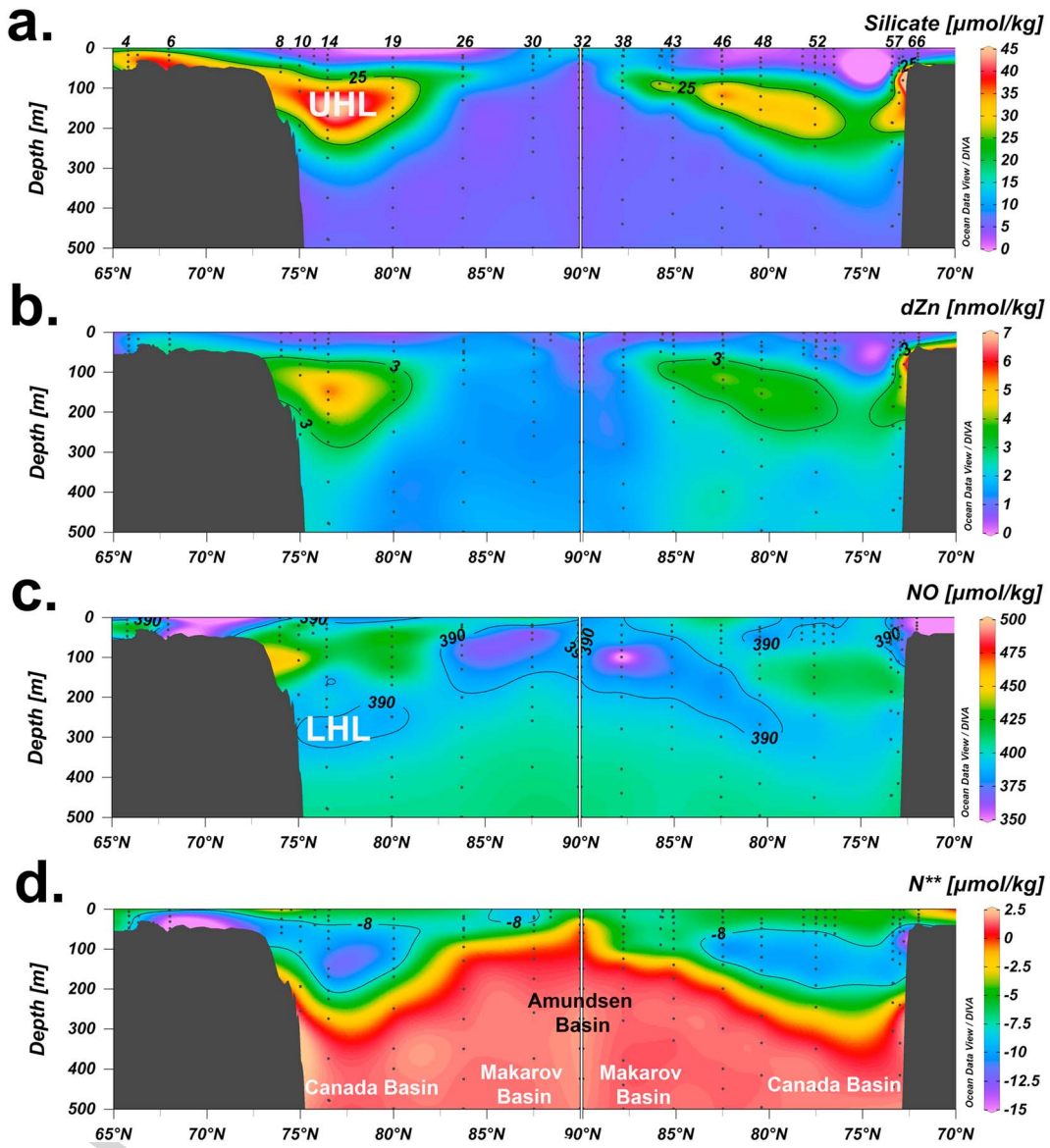

Figure 5. Upper 500 m of the northbound (left) and southbound (right) transects to characterize the halocline layers. (a) Si > 25 µmol/kg defines the Pacific-derived upper halocline layer (UHL; Anderson et al., 2013; Jones & Anderson, 1986; Macdonald et al., 1989). (b) Dissolved zinc with a contour of 3 nmol/kg to highlight the location of the UHL and tight correlation to Si. (c) The tracer NO with a contour <390 µmol/kg defines the Atlantic-derived lower halocline layer (LHL). (d) The tracer N** (Aguilar-Islas et al., 2013) indicative of Chukchi Shelf porewater denitrification fluxes with a contour of −8 µmol/kg in the UHL. Labels in (d) delineate the basin boundaries for the Makarov, Canada, and Amundsen Basins.

from Chukchi Shelf waters that have undergone brine rejection (Shimada et al., 2005; Woodgate et al., 2005). As Chukchi Shelf waters originate from incoming Pacific water, the UHL is best illustrated by a Si maximum centered on salinity 32.8 (Figure 5a). Here we characterize the UHL as having a [Si] > 25 µmol/kg (Anderson et al., 2013; Jones & Anderson, 1986; Macdonald et al., 1989), with a close correlation to dZn (Figures 5a and 5b). In contrast, the Canada Basin lower halocline layer (LHL: θ −1.5–0.3 °C, S 33.1–34.7) is composed primarily of Atlantic-origin water that shoals and picks up brine-rejected salt on the Eurasian shelf, eventually mixing with Pacific-origin water. Following previous work (Jones & Anderson, 1986), we characterize the LHL using a minimum in the conservative tracer NO (NO = $[O_2]$ + 9$[NO_3^-]$), indicative of a shelf origin for these waters (Figure 5c). It is immediately evident that while the UHL Si maximum is confined to the Canada Basin, the minimum in NO, centered at S = 34.6, is present in the Makarov and Amundsen Basins as well, albeit shallower and with lower salinity around 33 (Figures 4a and 5c). This supports the

idea that the LHL of the Canada, Makarov, and Amundsen Basins share a Eurasian shelf origin, although the exact continental shelf is likely unique in each case (Rudels et al., 1994, 2004).

The water mass known as the Atlantic layer, hereafter specified as Fram Strait Branch (FSB) water, lies below the halocline and originates from North Atlantic waters ($\theta > 3$ °C) that enter the Fram Strait and split into (1) a branch that travels to the west of Svalbard island, becoming the warmer, fresher FSB, and (2) a branch that loops eastward over the Barents Sea, becoming colder and saltier from shelf convection to form the deeper Barents Sea Branch (BSB; Schauer et al., 2002; Woodgate et al., 2001). Due to these different water mass histories, these two branches likely carry different biogeochemical signatures. The FSB mixes with the colder, less saline halocline layers above, losing temperature along the 27.9 isopycnal as it circulates counterclockwise through the Makarov and Canada Basins (Rudels et al., 1994; Schauer et al., 2002; Woodgate et al., 2001). The FSB ($\theta > 0$ °C, S 34.86) lies within the Makarov and Canadian Basins between 350 and 800 m (Figure 4). The underlying BSB ($\theta > -0.15$–0 °C, S 34.88) extends to 1,150 m.

Arctic deep waters (>1,200 m) originate in the far North Atlantic (Greenland and Norwegian Seas) and both enter and exit the Arctic through the Fram Strait (2,600-m sill). Radiocarbon data show Arctic deep water ages of ~250 years in the Eurasian Basin and ~350 years in the Amerasian Basin (Schlosser et al., 1997; Tanhua et al., 2009), with interbasin exchange restricted by the 1,870-m Lomonosov Ridge sill (Björk et al., 2007). However, the Makarov and Canada Basins are also separated by a 2,200-m sill in the Alpha-Mendeleev Ridge, leading to a mean deep water age of ~300 years for the Makarov and ~400 years for the Canada Basin (Tanhua et al., 2009; Timmermans & Garrett, 2006). These old, deep waters in the Western Arctic are also subject to mixing and continental slope fluxes as a result of brine rejection and dense water subduction during aging (Aagaard et al., 1985).

3.2. The sPML dZn Distribution

In the sPML (0–25 m) along GN01, dZn ranged 0.37–3.04 nmol/kg with an average of 1.06 ± 0.52 nmol/kg ($n = 63$). This is significantly higher than the global surface dZn average of 0.36 ± 0.48 nmol/kg (Schlitzer et al., 2018; $n = 187$). Within the North Pacific, this average increases slightly to 0.48 ± 0.40 nmol/kg [Kim et al., 2017]; $n = 27$), but even this is less than 50% of the mean surface dZn concentration of the Western Arctic. In addition to higher concentrations, surface dZn concentrations in the Western Arctic also show distinct spatial variations (Figure 6a), averaging 1.31 ± 0.81 nmol/kg over the Bering Shelf/Chukchi Shelf (Stations 2–6), decreasing to 0.84 ± 0.25 nmol/kg across the Chukchi Shelf break (Stations 8–14 and 5–66), and gradually increasing again to 1.11 ± 0.60 nmol/kg near the North Pole (Stations 30–43), compared with only 0.51 nmol/kg at our subarctic North Pacific (Station 1) site. In order to assess how Arctic sPML dZn distributions might be altered by future modifications of riverine fluxes, sea ice melt, and Arctic circulation (Markus et al., 2009; Overland & Wang, 2005; Peterson et al., 2002; Woodgate, 2018), a quantitative assessment of dZn provenance in the surface Arctic is required. Potential sources of dZn to the sPML include sea ice melt, riverine inputs, and Pacific water inflow modified by interaction with the continental shelves. F6

3.2.1. Sea Ice Inputs (Marginal Ice Zone)

Sea ice is thought to be a significant source of dZn to Arctic surface waters, based on total (unfiltered) Zn concentrations averaging 450 nmol/kg (Tovar-Sánchez et al., 2010). However, the concentration of dZn in sea ice during GN01 has been recently reported as much lower (3.12 ± 1.66 nmol/kg [Marsay et al., 2018]) suggesting a less significant source of dZn to the Western Arctic sPML than first hypothesized. In the present study, the fraction of water derived from sea ice melt (Fsim, Figure 6a) at MIZ stations (Stations 8–17 and 51–57) was quantified using $\delta^{18}O$, macronutrient, and salinity end members as well as the "Arctic N-P" tracer method described in Newton et al. (2013) for sea ice, meteoric water (river and precipitation, "Fmet"), and Atlantic and Pacific seawaters. When dZn is plotted against Fsim, a weak negative linear correlation ($r^2 = 0.45$) is evident at the MIZ stations (Figure 6b; Stations 8–9 excluded because of shelf influence). This indicates that sPML dZn concentrations are either (1) diluted by sea ice melt and/or (2) coincidentally decreased at MIZ stations because of biological uptake of dZn in the surface, which is a primary driver of low-surface dZn globally (Bruland, 1980; Croot et al., 2011; Lohan et al., 2002), or (3) diluted by Beaufort Gyre water (discussed below). If the removal of Zn was primarily biological, one might expect to find a negative relationship between dZn and the pigment chlorophyll *a* (chl*a*; Jakuba et al., 2012; Wyatt et al., 2014), a known tracer of phytoplankton biomass. Since no such relationship was observed ($r^2 = 0.003$ data not

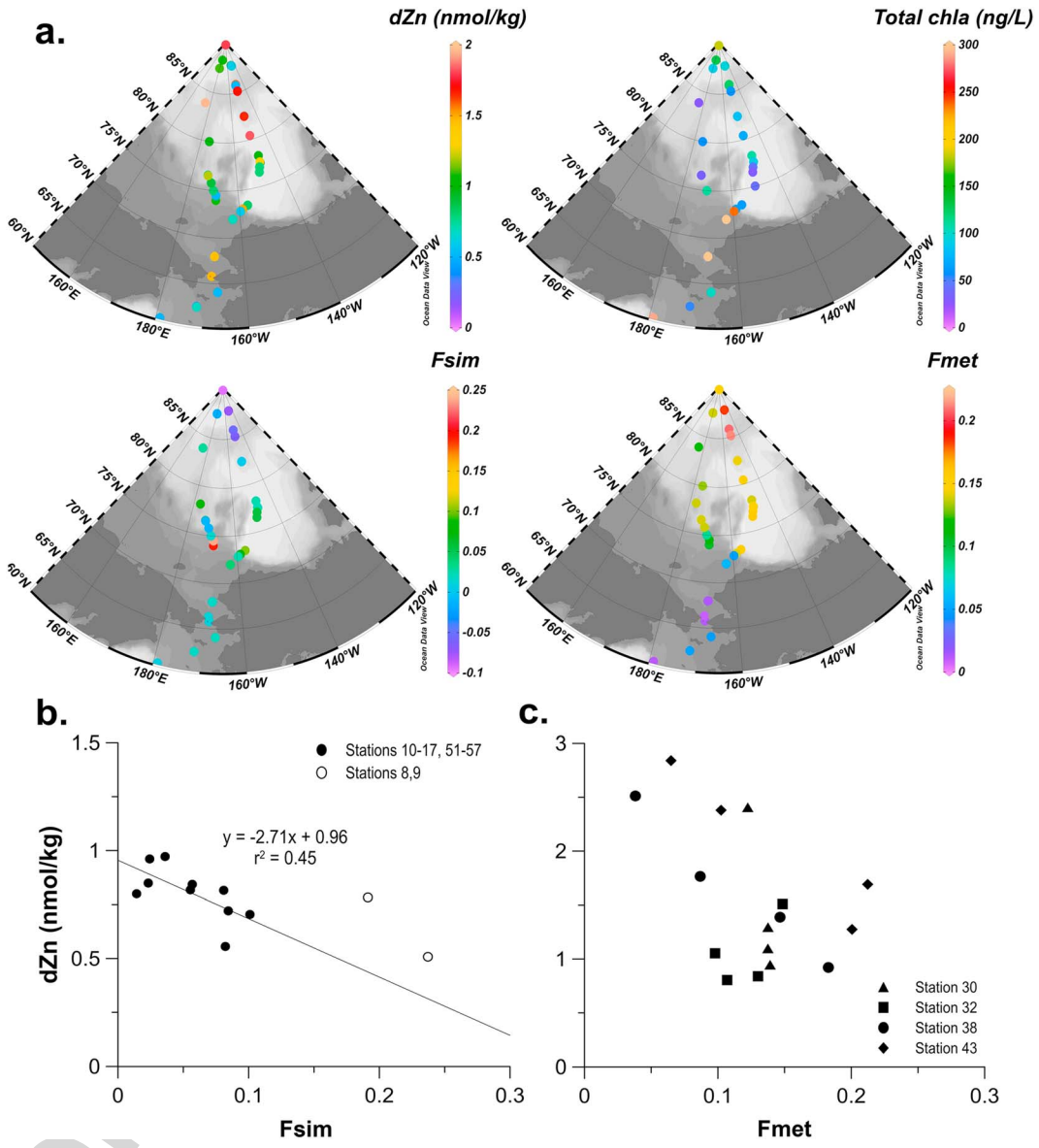

Figure 6. Characterization of dissolved zinc (dZn) in the surface Polar Mixed Layer (0–25 m). (a) Isosurface plots of dZn, total chlorophyll *a* (chl*a*), fraction of sea-ice melt (Fsim), and fraction of meteoric water (Fmet); (b) dZn versus Fsim at stations in the MIZ with an inverse correlation indicating dilution of dZn in seawater by sea-ice melt where shelf-influenced Stations 8 and 9 were removed; and (c) dZn versus Fmet in the upper 80 m at transpolar drift-influenced stations. There appears to be no clear meteoric water influence on dZn at these stations, despite the high dZn concentration in Siberian rivers (Hölemann et al., 2005).

shown), mixing with low-dZn sea ice melt was more likely the dominant control on dZn concentrations within the MIZ.

In fact, biological uptake of dZn during GN01 was largely insignificant in the central Arctic away from the productive shelves. Isosurface views of chl*a* (Figure 6a) show high values on the Chukchi Shelf (chl*a* up to 12.8 μg/L) and oligotrophic conditions off-shelf (Stations 10–60 chl*a* < 0.2 μg/L), indicating that offshore primary production exerts little control on sPML dZn distributions. Together, the Chukchi Shelf and Bering Strait/Shelf are the most productive in the Arctic (Sakshaug, 2004), and biological uptake of dZn likely occurs in surface waters of these shelves such that residual low-surface dZn concentrations can be transported offshore to open Arctic sPML waters. In fact, the increasing sPML dZn concentrations moving from the Chukchi shelf (<1 nmol/kg) to the open Arctic (>1 nmol/kg; Figure 6a) suggest not only negligible

biological uptake in the central Arctic but require sources of dZn to the sPML via mixing from the halocline below or via external dZn sources, as discussed next.

3.2.2. River and Precipitation Inputs

Rivers are known to be an important source of freshwater to the Arctic Ocean with over 3,300 km^3 of freshwater supplied annually (Aagaard & Carmack, 1989), most of which comes from the Yukon, Mackenzie, Ob, and Yenisey Rivers (Figure 1). Arctic riverine flux has increased by 7% between 1936 and 1999 as a result of climate change (Peterson et al., 2002), leading to changes in nutrient fluxes and Arctic stratification (Macdonald et al., 1999, 2015). Along the GN01 transect, Stations 2 and 3 were chosen to characterize potential Yukon River outflow (Figure 1). The fraction of meteoric water (Fmet, Figure 6a), which includes a combination of riverine and precipitation-sourced freshwaters, at the surface was elevated to 5% compared to nonriverine Stations 4–6 (<1%), but even 5% Fmet was low compared to central Arctic stations (e.g., Stations 30–43) in the path of the transpolar drift (TPD), where Fmet consistently exceeded 10% in the surface. The low Fmet at Stations 2–3 likely occurs because they are located outside the path of the coastal current that carries Yukon River water northward along the Alaskan coast (Li et al., 2017). Accordingly, there was no significant correlation between Fmet and dZn at these two stations (data not shown). While the Mackenzie River outflow lies outside of our transect, it is known to contribute freshwater to the Beaufort Gyre and Canada Basin (Macdonald et al., 1999).

Offshore from the Chukchi Shelf, freshwater injections into the central Arctic are evident, particularly from a decrease in salinity and depression of isopycnals along both transects (>75°N), likely originating in the Beaufort Gyre (Proshutinsky et al., 2002). North of 85°N, Fmet increased (13–22%) toward the North Pole (Stations 30–43, Figure 6a), indicating the presence of riverine- and/or snow-sourced meteoric freshwaters derived from the well-known TPD (Kadko et al., 2016; Rudels, 2015; Rutgers van der Loeff et al., 2012). As described previously, an enrichment in sPML dZn concentration was also observed at these stations (1.11 ± 0.60 nmol/kg). However, the absence of a significant correlation between dZn and Fmet in the upper 80 m ($r^2 = 0.20$, Figure 6c) suggests that the TPD is not the source of dZn.

If not rivers, then what explains the apparent increase in dZn north of 85°N? We argue that it is (1) not actually an increase in dZn but, instead, an "apparent enrichment" accentuated by the MIZ sea ice melt and Beaufort Gyre freshwater dilution of surface dZn at 70–80°N, (2) influenced somewhat by vertical mixing with the dZn enriched, shallow Makarov Basin halocline (80- to 100-m depth; discussed below), and (3) at least somewhat facilitated by transport of Chukchi Shelf-derived dZn enrichments (discussed in section 3.3 below). Thus, we conclude here that rivers themselves do not appear to be a major source of dZn to the open Arctic.

3.2.3. Continental Shelf/Pacific Inputs

Along the Bering and Chukchi shelves (Stations 2–8 and 61–66), dZn concentrations in the upper 80 m were elevated, ranging between 0.37 and 6.49 nmol/kg with the lowest concentrations associated with PML water at the shelf break (MIZ dilution by low-dZn sea ice melt) and the highest concentrations located in near-bottom waters of the shelf (Figure 5b). This clearly indicates an enrichment of dZn along the Bering and Chukchi shelves. Three potential sources of dZn to the continental shelf are (1) incoming North Pacific waters, (2) authigenic dZn sources from shelf sediments, and/or (3) shelf remineralization inputs.

We note that while we have scant sample coverage of the Bering Strait and Chukchi Shelf, dZn concentrations were most elevated in bottom waters of the Chukchi Shelf (>6 nmol/kg; Figure 7) where there is a known benthic source of up to 13-nmol/kg dZn in near-sediment bottom waters (Cid et al., 2012) concurrent with decreased light transmission resulting from resuspended sediments (Gardner et al., 2018). Following this, we hypothesized a sediment-derived source of dZn to these shelf waters as they enter from the North Pacific and traverse the margin, discounting the hypothesis that these dZn enrichments are Pacific-derived. In support of this, the Zn:Si linear regression slope for the Bering Strait and Bering/Chukchi Shelves of 0.076 ± 0.012 nmol/μmol (Figure 7a) is higher than that for the upper 100 m of the North Pacific (Station 1, 0.052 ± 0.012 nmol/μmol), the regression slope for the central subarctic North Pacific (0.053 nmol/μmol; Kim et al., 2017), and the global GEOTRACES data set (0.0596 ± 0.0003 nmol/μmol; Schlitzer et al., 2018), suggesting Zn:Si enrichment in the Chukchi Shelf sediments. F7

A shelf sediment dZn flux could be derived from authigenic minerals or remineralization of biogenic particles. Dissolved Si also showed a strong maximum in bottom waters of the Bering Strait and Chukchi Shelf,

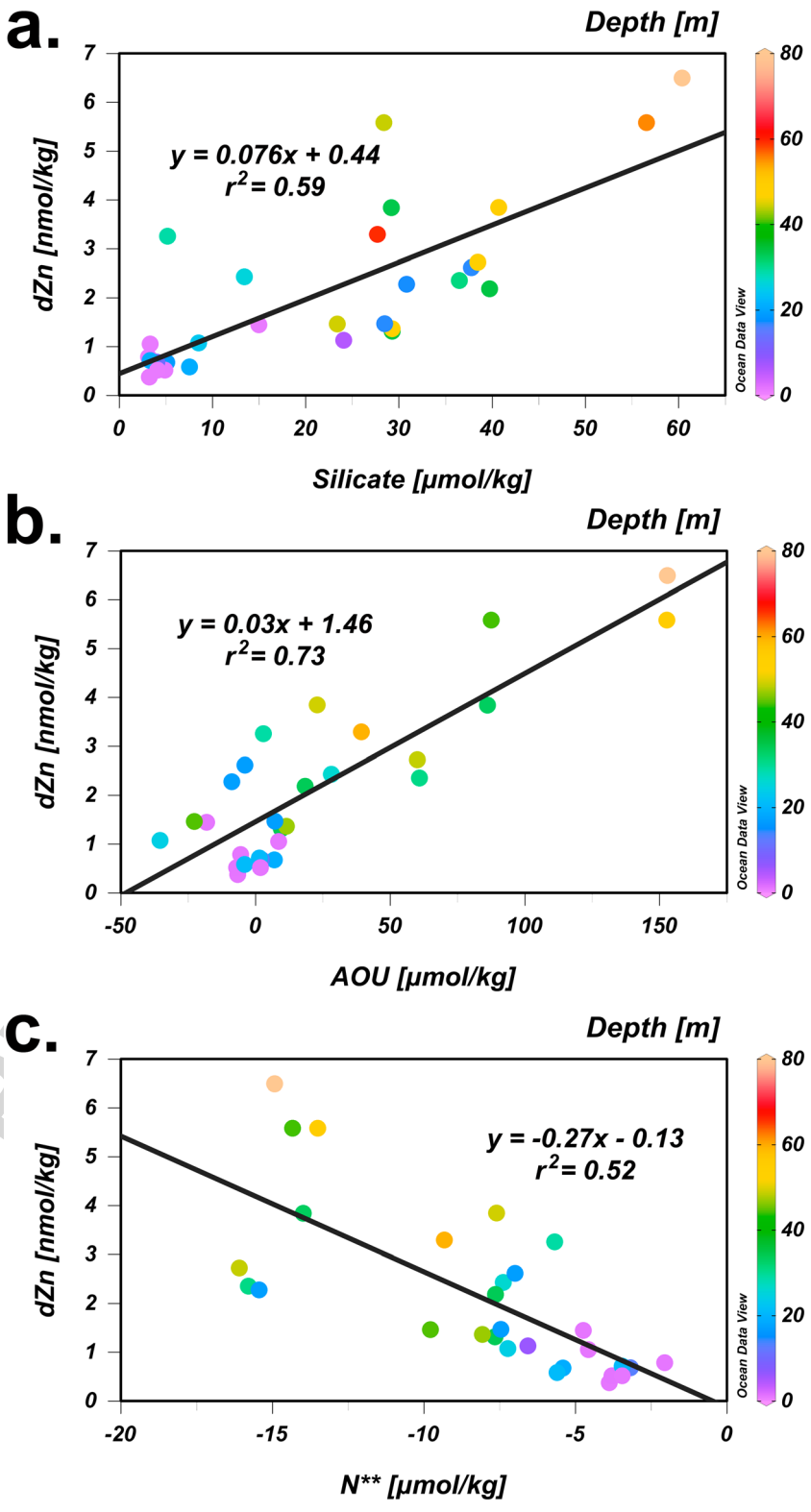

Figure 7. Chukchi Shelf (Stations 2–8 and 61–66) correlation between dZn and (a) Si (µmol/kg) to show a remineralized nutrient source, (b) apparent oxygen utilization (AOU) to confirm a remineralization source, and (c) N** to show a remineralization source constrained to the sediments. The color bar indicates depth along the shelf (maximum 80 m), and we note that remineralization signals are greatest at deepest depths, indicating a porewater remineralization source.

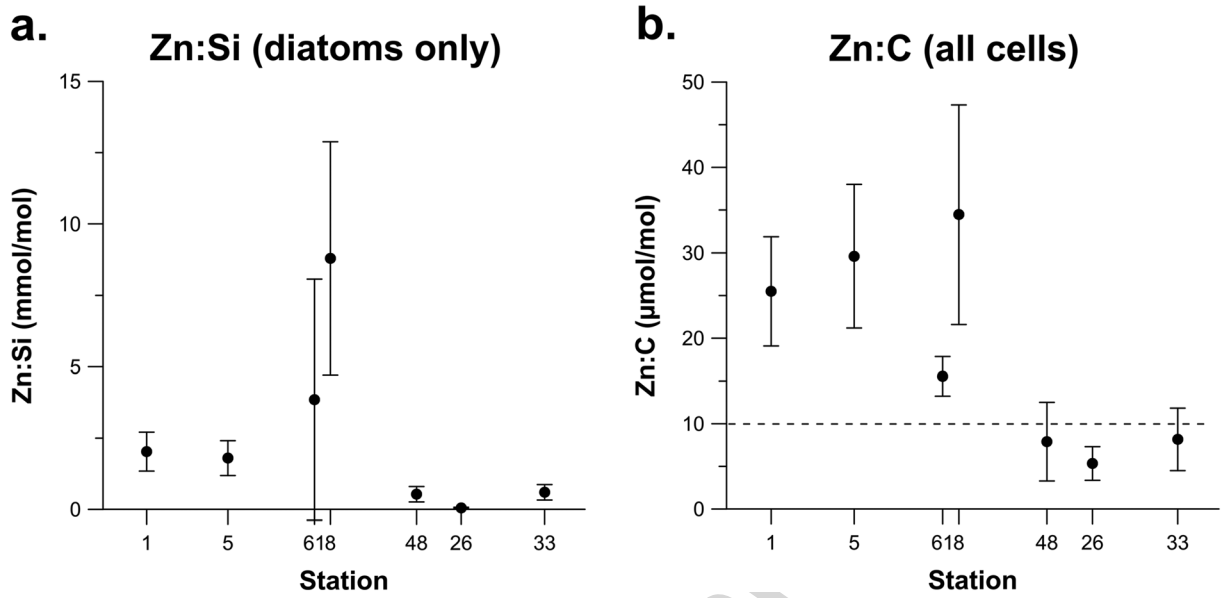

Figure 8. (a) The geometric mean Zn:Si ratios determined by synchrotron X-ray fluorescence analyses in diatoms only (with associated standard error), (b) The geometric mean Zn:C ratios determined by SXRF in all cells (with associated standard error). The dotted line represents previous phytoplankton net-tow measurements compiled from (Bruland et al., 1991). Both plots include the North Pacific (Station 1), on-shelf stations (5, 8, and 61) and off-shelf stations (26, 33, and 48) plotted in order of increasing latitude. Notably, Zn:Si and Zn:C ratios are higher along the shelf compared to the off-shelf stations.

reaching 61 µmol/kg compared with 25 and 14 µmol/kg north of the Chukchi Shelf along the northbound and southbound lines, respectively (Figure 5a), suggesting some sediment dZn source rather than an authigenic source. Authigenic Zn sulfides can precipitate in low-O_2, sulfidic porewaters, and if these Zn sulfides form in the colloidal fraction, they may provide a sedimentary source of dZn (Conway & John, 2015; Trefry et al., 2014). However, we find this unlikely given that Chukchi Shelf upper sediments are rarely and only sparingly sulfidic (Gobeil et al., 2001). Finally, we also observed a benthic maximum in apparent oxygen utilization (AOU), a tracer for biological respiration, and a positive linear regression between AOU and dZn (0.030 ± 0.004 nmol/µmol, r^2 = 0.73) within Chukchi Shelf waters (Figure 7b), further supporting a sediment remineralization source of dZn to shelf bottom waters concurrent with opal dissolution.

Our hypothesized sediment remineralization source of dZn was reinforced by measured cellular stoichiometry in Chukchi Shelf waters, showing elevated Zn:Si and Zn:C ratios in cells compared to a global compilation of cellular data (Twining & Baines, 2013). Zn:Si within diatoms in Chukchi Shelf waters (Stations 5, 8, and 61) averaged 4.8 ± 3.6 mmol/mol (geometric mean ± SD of station geometric means), which is higher than the North Pacific (Station 1) value of 2.0 ± 0.7 mmol/mol (Figure 8a). Zn:C within all analyzed phytoplankton cells along the same shelf stations averaged 26.5 ± 9.8 µmol/mol compared to 11.7 ± 9.3 µmol/mol off-shelf and in lower-latitude oligotrophic communities (Figure 8b; Twining et al., 2011; Twining et al., 2015). This suggests a clear enrichment of dZn compared to C and Si in phytoplankton cells along the Chukchi Shelf. We postulate that the elevated cellular Zn:C in Chukchi Shelf phytoplankton likely results from increased dZn availability and uptake compared with the central Arctic, as previously observed for the highly productive California Shelf region (Twining, 2018). F8

Critically for the Arctic dZn cycle, we hypothesize that once the shelf phytoplankton deposit their elevated Zn:Si and Zn:C as phytodetritus in the shallow shelf sediments, sedimentary remineralization of the organic tissue of those cells would supply a Zn-rich dissolved nutrient flux back into shelf waters, effectively increasing the Zn:macronutrient ratios observed in the water column. This sedimentary dZn flux might be accentuated compared to Si due to the preferential remineralization of "soft" tissues containing Zn and C over the "hard" Si tests, as demonstrated by decreasing cellular Zn:Si ratios with depth in the subtropics (Twining et al., 2014) and in the 1,000-fold lower Zn:Si ratio of sedimentary frustules (Andersen et al., 2011; Ellwood & Hunter, 1999; Hendry & Rickaby, 2008) compared with the water column phytoplankton in Arctic shelf waters.

To test this hypothesis, we compared our phytoplankton cellular Zn:C with estimated Zn:C derived from our water column dZn:AOU regression analyses using a Redfield O:C of 170:117 (Anderson & Sarmiento, 1994). Over the Chukchi Shelf, the Zn:AOU regression slope of 0.030 ± 0.004 nmol/μmol) yielded an estimated Zn:C of 43 ± 6 μmol/mol. This value is well within the range of median Zn:C cellular stoichiometries from the shelf stations (13–75 μmol/mol). We note that there is significant intrapopulation variability associated with single-cell measurements (i.e., SXRF, nanoSIMS, and flow cytometry), and multiple approaches can be taken to estimate average population stoichiometry. The arithmetic mean Zn:C for shelf station phytoplankton populations was 57 μmol/mol, above the calculated Zn:C from water column remineralization.

Regardless of the metric used, Zn:C cellular stoichiometries for shelf phytoplankton (13–75 μmol/mol) are elevated above offshore cellular Zn:C (4–6 μmol/mol), strengthening our argument that the dZn enrichments in Chukchi Shelf bottom waters are derived from "soft" tissue remineralization of high-Zn:C phytoplankton. In addition, the geometric mean cellular Zn:Si ranged 2–9 mmol/mol along the shelf, which is 2 orders of magnitude higher than the dissolved water column slope of 0.076 mmol/mol. If dZn and C are preferentially remineralized over Si in the water column, this would elevate the Zn:Si of the water column through the Bering Strait and Chukchi Shelf. However, these waters are regularly resupplied by incoming Si-rich North Pacific waters with a lower Zn:Si slope of 0.052 nmol/μmol, only allowing moderate elevation of Chukchi shelf Zn:Si slopes over their source ratios.

Additionally, to support our conclusion that the remineralization of these Zn-enriched phytoplankton is occurring in the upper sediment porewaters of the shelf instead of in the water column, we point to the chemical tracer N** (Figure 5d). Negative values of this parameter, defined as (0.87([DIN] – 16[PO_4^{3-}] + 2.9) μmol/kg), where DIN is the sum of nitrate and nitrite, are a tracer of porewater denitrification and/or anammox in the Chukchi and Bering shelves, since water column dissolved oxygen concentrations (>240 μmol/kg) above these shelves are far too high to enable water column dentrification (Aguilar-Islas et al., 2013; Nishino et al., 2005). During GN01, over both shelves (Stations 2–8 and 61–66) there was a significant negative correlation between dZn and N**, indicating a similar porewater remineralization source for both variables (Figure 7c).

Thus, to conclude, PML surface waters of the Arctic have elevated dZn concentrations compared to other ocean global basins. The elevated dZn is primarily due to nutrient-rich incoming Pacific waters that receive further dZn-rich fluxes from the sediment porewater remineralization of deposited high Zn:C and Zn:Si phytoplankton cells over the Bering and Chukchi shelves; these high-dZn shelf bottom waters form the subsurface halocline offshore, which is discussed next. The lower-dZn sPML waters over the shelf are eventually advected offshore into the Canada Basin by local currents (Corlett & Pickart, 2017; Pickart et al., 2005), where they appear to be at least seasonally diluted by low-Zn sea ice melt at the shelf break, despite high concentrations of total Zn in ice cores from the literature (Tovar-Sánchez et al., 2010). While Arctic rivers do contain substantial dZn (Hölemann et al., 2005), the correlations between dZn and Fmet near both the Yukon outflow and in the path of the TPD reject the hypothesis of major riverine dZn sources to the central Arctic. Instead, elevated dZn in the open Arctic PML primarily results from mixing up of shelf-derived porewater inputs following the remineralization of Zn-rich phytoplankton, as well as limited biological uptake of dZn under the ice.

3.3. Halocline Zn Distribution

The most prominent feature of the Western Arctic dZn distribution (Figure 5b) is the subsurface maximum in the Canada Basin (110–200 m) with concentrations ranging from 3.62–6.59 nmol/kg (average 4.39 ± 0.88 nmol/kg). The salinity range of 31–33.1 designates these waters as the UHL (Figure 4a). The magnitude of this UHL dZn maximum agrees well with data from prior studies near the Chukchi Shelf break (Cid et al., 2012; Kondo et al., 2016). In the Makarov Basin (Stations 26, 30, and 38), this halocline feature is also present but is shoaled to ~80 m and is lower in concentration at 2.59 ± 0.24 nmol/kg. Using the [Si] > 25 μmol/kg tracer (Figure 5a) to trace this feature, we see that Si concentrations reach ~50 μmol/kg and coincide with the dZn maximum. The Zn:Si slope in the UHL is 0.110 ± 0.010 nmol/μmol (r^2 = 0.90), much higher than the North Pacific Zn:Si slope of 0.052 ± 0.012 nmol/μmol (Station 1, to 100 m), suggesting an additional source of excess dZn to the Arctic halocline beyond that advected from the North Pacific.

The Zn:Si slope increases along its transport path from 0.052 ± 0.012 nmol/μmol in the Bering Sea (Station 1) to 0.076 ± 0.012 nmol/μmol along the Chukchi and Bering shelves (Stations 2–3 and 61–66) to 0.110 ± 0.010 nmol/μmol in the subducted UHL. As discussed above, the increase in the Zn:Si regression slope moving from the Bering Sea over the Chukchi shelf is due to the preferential remineralization of Zn and C in "soft" tissues sourced to the incoming nutrient-rich North Pacific waters. But why do the Zn:Si regression slopes continue to increase from the shelf to the UHL? The UHL forms from the bottommost brine-rejected waters of the shelf, which should carry elevated Zn:Si ratios due to the preferential remineralization of Zn compared to Si in sediment porewaters (see section 3.2.3 above). This shelf porewater influence on the UHL can be seen by the correlation of dZn with the sediment-derived N** minimum, which also extends offshore into the UHL (Figure 5d). We also observed the same Zn:AOU relationship in the UHL (0.029 ± 0.003 nmol/μmol, $r^2 = 0.65$) as we do in the Chukchi Shelf water column (0.030 ± 0.004 nmol/μmol, Figure 7b), both leading to Zn:C ratios of 42–43 μmol/mol that match the cellular stoichiometry of shelf phytoplankton as described above, reinforcing the dominance of "soft" tissue remineralization of dZn. In fact, given the low cellular Zn:C stoichiometries (<10 μmol/mol) for phytoplankton in offshore stations, this Zn:AOU relationship in the UHL can only be derived from cells with higher cellular Zn:C, as on the Chukchi Shelf.

It is worth mentioning that the northbound and southbound distributions of dZn in the UHL are distinctly different (Figure 5b). In particular, a point source for dZn at Station 14 at 150 m can be attributed to an eastward moving eddy (acoustic Doppler current profiler data not shown), a common mode of transport for Pacific-origin water advected rapidly off-shelf (Pickart et al., 2005). Recent findings suggest that Pacific water does not flow uniformly offshore from the Chukchi Shelf (Brugler et al., 2014; Corlett & Pickart, 2017). The eastern Chukchi Shelf Stations 57–66 are more affected by shelf break jets traveling eastward from Herald canyon, while the more western Stations 8–10 are further north and are affected by the westward Chukchi slope current.

In contrast to the UHL, the dZn concentrations of the Canada Basin LHL, as well as the haloclines of the Makarov and Amundsen Basins, were lower (2.44–4.28 nmol/kg) with lower slopes of Zn:Si (0.057 ± 0.008 nmol/μmol). The LHL dZn appears to be controlled by mixing between the overlying dZn-rich UHL and the underlying dZn-poor Atlantic layer (discussed below). In fact, a plot of dZn concentrations versus conservative θ is linear between the core of the FSB Atlantic layer (at the depth of maximum θ) and the core of the UHL (at the depth of maximum dZn; Figure 9a). While the T-S signature shows the intrusion of the slightly colder and saltier Eurasian-formed LHL waters, dZn appears to result simply from mixing, without additional Eurasian shelf supply. Thus, a critical question remains: If all Arctic halocline layers are formed from brine rejection on Arctic shelves that could produce excess dZn inputs from shelf sediments, then why is the Pacific/Chukchi UHL particularly enriched in dZn, while LHL waters formed on Eurasian shelves are not? In the case of the Barents Sea, no evidence has been found of nutrient-rich water emanating from the St. Anna Trough (Anderson et al., 2013). Brine-rejected waters also contact the sediment surface of the Eurasian Shelf, but much of the Eurasian Shelf (e.g., the Barents Sea) is deeper, in which case more of the phytoplankton would be remineralized in the water column, preventing such a significant porewater remineralization flux as observed in the shallow Chukchi Shelf.

In summary, the highest dZn concentrations along the entire GN01 transect were found in the Chukchi Shelf-derived UHL. Notably, the Canada Basin LHL (designated by a minimum in NO), and to some extent the Makarov and Amundsen haloclines, showed much lower dZn (Figure 9b), despite the fact that this halocline is also formed on other (Eurasian) shelves. Thus, Chukchi Shelf and slope sediments appear to be unique in delivering a dZn enrichment to its overlying PML water column and downstream UHL, through a combination of high productivity, active remineralization of high Zn:C cells in shelf sediments, and shallow Chukchi Shelf depth where brine rejected waters contact the sediments.

3.4. Atlantic Layer: FSB

Below the Western Arctic Ocean halocline is the Atlantic layer, primarily composed of the warm (θ > 0 °C) FSB between 350 and 800 m (Figure 4b; Coachman & Barnes, 1963; Timofeyev, 1962). The FSB waters slowly lose their heat (θ maximum attenuated) through mixing with overlying cold halocline waters as they circulate cyclonically from the Amundsen to Makarov to Canada Basin along their known flow path (Rudels et al., 1994). Dissolved Zn in the FSB θ maximum ranged 1.24–3.59 nmol/kg throughout the three basins

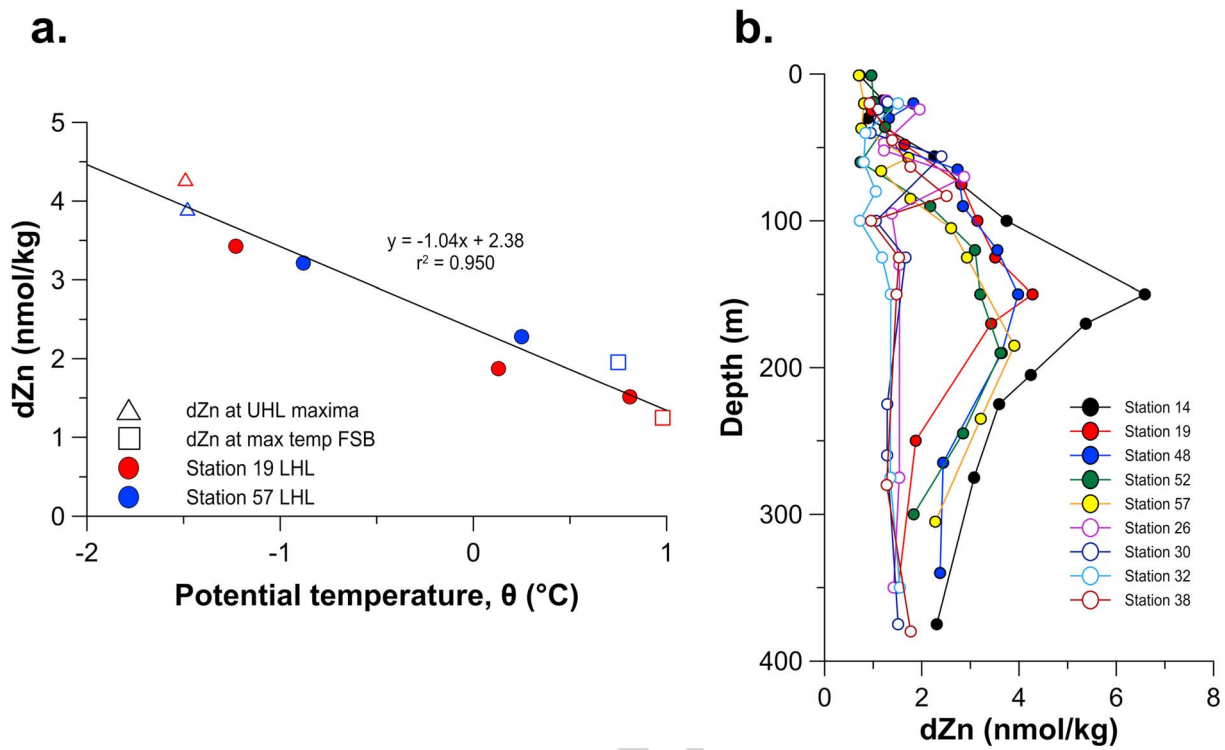

Figure 9. (a) Dissolved zinc (dZn) versus potential temperature demonstrating that the lower halocline layer (LHL) dZn concentrations (filled dots) are formed from mixing between the upper halocline layer (UHL) dZn maximum (triangles) and the Atlantic layer (Fram Strait Branch [FSB], squares) end members at two representative Canada Basin stations (19 and 57); (b) dZn depth profiles at select stations in the Makarov (26–38) and Canadian (14, 19, and 48–57) basins demonstrating a UHL dZn peak between 100 and 200 m that shoals in the Makarov to 50–80 m and is virtually absent in the Canadian LHL 250–450 m.

sampled on GN01. This range is consistent with published dZn concentrations in the Atlantic layer of stations sampled previously off the Chukchi Shelf (Kondo et al., 2016).

In other ocean basins at these intermediate depths, we would expect to see a nutricline, representing a combination of preformed and in situ vertical remineralization inputs of nutrients including dZn. Instead, in the FSB there is a sharp decrease in dZn concentrations with depth (Figure 3). In the absence of significant biological production under the central Arctic ice (Arrigo et al., 2003), we hypothesized that this gradient was a product of water mass mixing between the dZn-rich halocline above and the incoming low-dZn FSB.

Maximum potential temperature (θmax) is a conservative tracer of the FSB, and we found a positive relationship between θmax and dZn ($r^2 = 0.80$; Figure 10b), which suggests that Western Arctic FSB dZn concentration gradients are derived from conservative mixing alone, while vertical regeneration inputs of dZn to FSB waters are negligible. Similarly, mixing was sufficient to predict subsurface dZn concentrations in the subtropical North Atlantic (Roshan & Wu, 2015), reinforcing the fact that mixing of dZn across water masses can be a significant driver of intermediate water dZn. To further emphasize the lack of regenerative dZn inputs to FSB waters, we also examined the respiration tracer AOU in the FSB. At the θmax of each station, dZn and Si both show a linear relationship with AOU (data not shown), typically indicating remineralization fluxes. However, AOU and θmax also have a linear relationship ($r^2 = 0.88$; Figure 10c), indicating that even AOU is conservatively mixed in the FSB layer of the Western Arctic and as such does not trace in situ remineralization. F10

We note that Station 32 (Amundsen Basin) falls off the mixing line (Figures 10b and 10c) due to its younger age. FSB waters feeding the Western Arctic spend time along the Laptev Sea continental slope where they are cooled by mixing as compared to the FSB branch of the Amundsen Basin (Jones et al., 1998; Rudels et al., 1994; Figure 10a). Additionally, Station 10 falls off the mixing line due to elevated AOU from the Chukchi Shelf. By extrapolating the θmax-dZn linear relationship to the core θ of FSB waters at the continental slope of the Laptev Sea, ~1 °C, we estimate the "preformed" dZn concentration that enters the

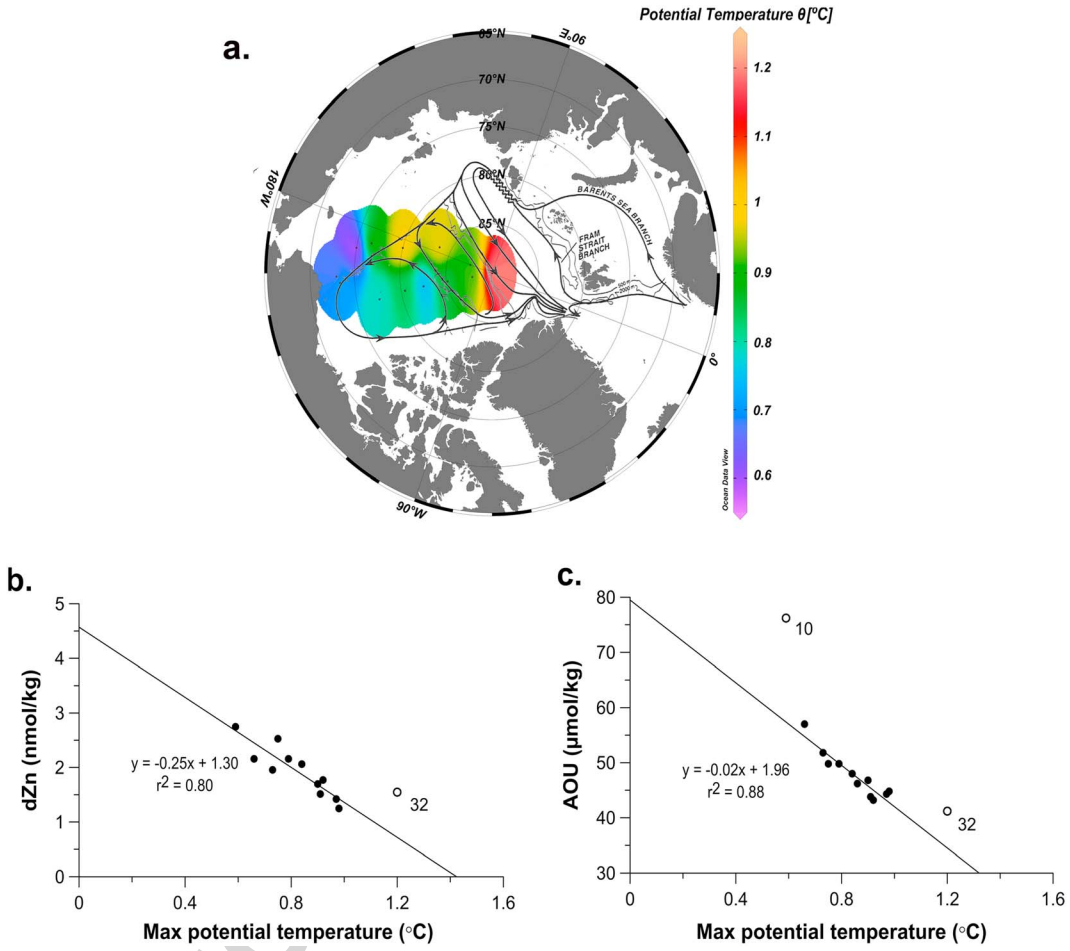

Figure 10. Intermediate Atlantic layer dZn dynamics. (a) An isosurface plot of max potential temperature at every station demonstrating the conservative temperature attenuation that follows the overlaid Atlantic layer circulation (Rudels et al., 1994). (b) Dissolved zinc (dZn) and (c) apparent oxygen utilization (AOU) versus the maximum potential temperature at every station, illustrating conservative mixing of dZn, instead of regenerative dZn inputs, in the Atlantic layer Fram Strait Branch. Station 32 was removed in (b) and (c) as an outlier for temperature due to its location in the Eurasian Basin, while Station 10 was removed in (c) given its close proximity to the Chukchi Shelf.

Western Arctic in the intermediate FSB Atlantic layer as ~1.3 nmol/kg. This relationship confirms that the dZn concentrations in the FSB layer arise from conservative mixing with the overlying, dZn-rich UHL during water mass aging, which raises the dZn concentrations and decreases the θ of FSB waters in the Western Arctic.

3.5. Arctic Deep Water

Below 1,000 m, dZn had uniformly low concentrations (1.27 ± 0.29 nmol/kg; Figure 11) compared to global deep water data from the North Atlantic (1.78 ± 0.44 nmol/kg) and North Pacific (9.82 ± 0.65 nmol/kg; Figure 3; Schlitzer et al., 2018). We explore two potential sources/sinks of dZn to/from deep waters (hydrothermal vents and bottom suspended particle nepheloid layers) and then investigate the cause for the low deep water dZn concentrations in the Arctic by comparing dZn across the Arctic Basins sampled during GN01. **F11**

3.5.1. Hydrothermal Vents

Recent literature suggests that hydrothermal vents may supply dZn to deep waters of the South Pacific (Roshan et al., 2016). The Gakkel Ridge (Figure 1) is a known location of hydrothermal activity in the Arctic Ocean (Edmonds et al., 2003), and there is evidence that hydrothermally influenced waters can be traced toward the Western Arctic using dFe and dMn distributions, even reaching the Amundsen Basin (Klunder et al., 2012; Middag et al., 2011). Along GN01, Station 32 in the Amundsen Basin is the

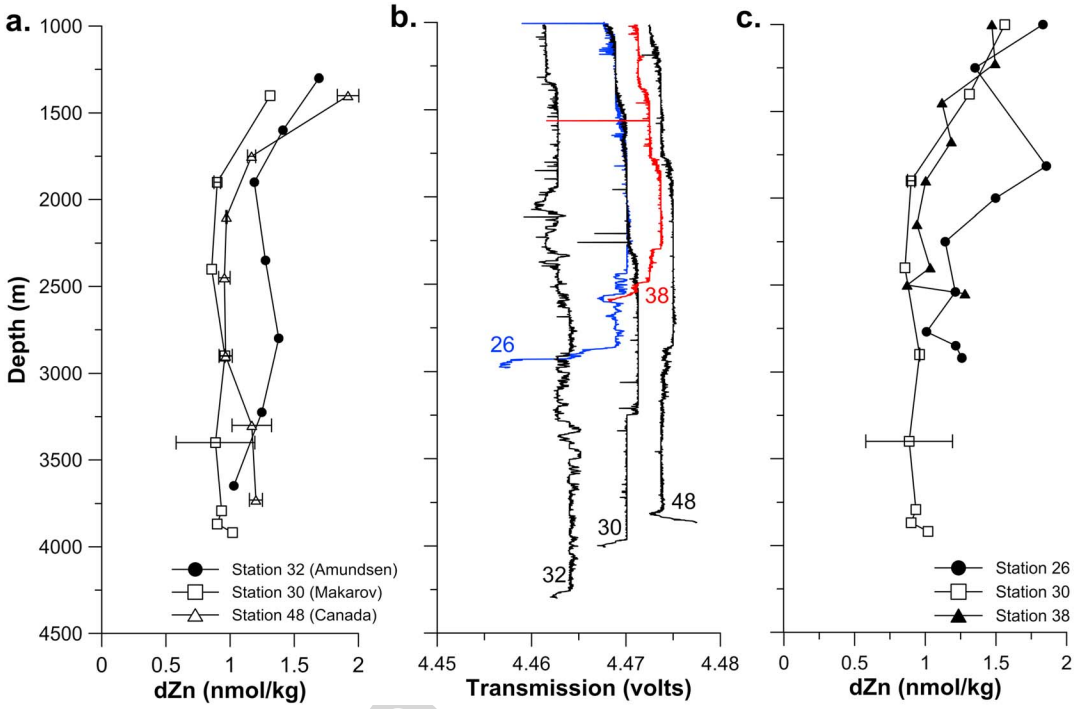

Figure 11. Arctic deepwater dZn. (a) Dissolved zinc (dZn) below 1,000 m where Station 32 (Amundsen Basin) shows a slight peak at 2,800 m compared to Stations 30 (Makarov Basin) and 48 (Canada Basin), which may be derived from hydrothermal fluxes; (b) light transmission data from the GTC CTD transmissometer, showing potential benthic nepheloid layer particles causing light attenuation at Stations 26, 30, and 38 (color to differentiate) and potential hydrothermal particles 2,000- to 2,500-m depth at Station 32 as well as a lack of hydrothermal particles at Station 48; (c) dZn below 1,000 m at stations where there was a benthic source of dZn coincident with low transmissometry. Error bars are included on plots where replicate analyses were available.

easternmost station, and thus, we have no samples from near the Gakkel Ridge to prove or disprove a hydrothermal source of Zn in the Arctic. Most water in the Amundsen Basin is of Atlantic origin, with potential inputs from brine rejection on the Barents Shelf (Jones, 2001). However, Station 32 shows a slight increase in dZn at depths 2,000–3,700 m with a broad maximum centered at 2,800 m (Figure 11a). Beam transmission at these depths do not confirm or deny a distal hydrothermal signal (Figure 11b). This 2,800-m dZn maximum at the North Pole is only slightly deeper than the 2,500-m hydrothermal peak observed for dFe in the Amundsen Basin by Klunder et al. (2012) and is unique to the Amundsen Basin, as profiles from the Makarov (Station 30) and Canada (Station 48) Basins do not show deep water dZn maxima (Figure 11a). Further confirmation of hydrothermal influence awaits measurement of conservative hydrothermal tracers, namely, ^{3}He, from GN01.

3.5.2. BNLs

Suspended particle benthic nepheloid layers (BNLs), typically identified by a reduction in light transmission from the CTD transmissometer (Gardner et al., 2018), are known to variably supply and/or remove dissolved trace elements and isotopes such as Fe, Al, Ti, Th, Pb, Nd, Ni, and Co from the water column (Fitzsimmons et al., 2015; Middag et al., 2015; Noble et al., 2017; Ohnemus & Lam, 2015; Rutgers van der Loeff et al., 2002). Recent analyses of transmissometry data (Gardner et al., 2018) suggest that along GN01, BNLs were present in the Western Arctic but dropped off substantially in thickness and particle concentration seaward of the Chukchi Shelf. At Stations 26, 30, and 38 in the Makarov Basin, we see small elevations in dZn at bottom depths (Figure 11c) where the light transmission is also reduced (Figure 11b). This suggests a small source of dZn ($\leq$0.3 nmol/kg) associated with resuspended material in the deep waters of the Makarov Basin. While Stations 48 and 57 within the Canada Basin also show slight enrichments in dZn in the bottom waters, they are not concurrent with decreased light transmission. Overall, while these data may reflect BNL sources, we emphasize that this dZn source is much smaller in magnitude than the dZn enrichments of the shelf-derived halocline.

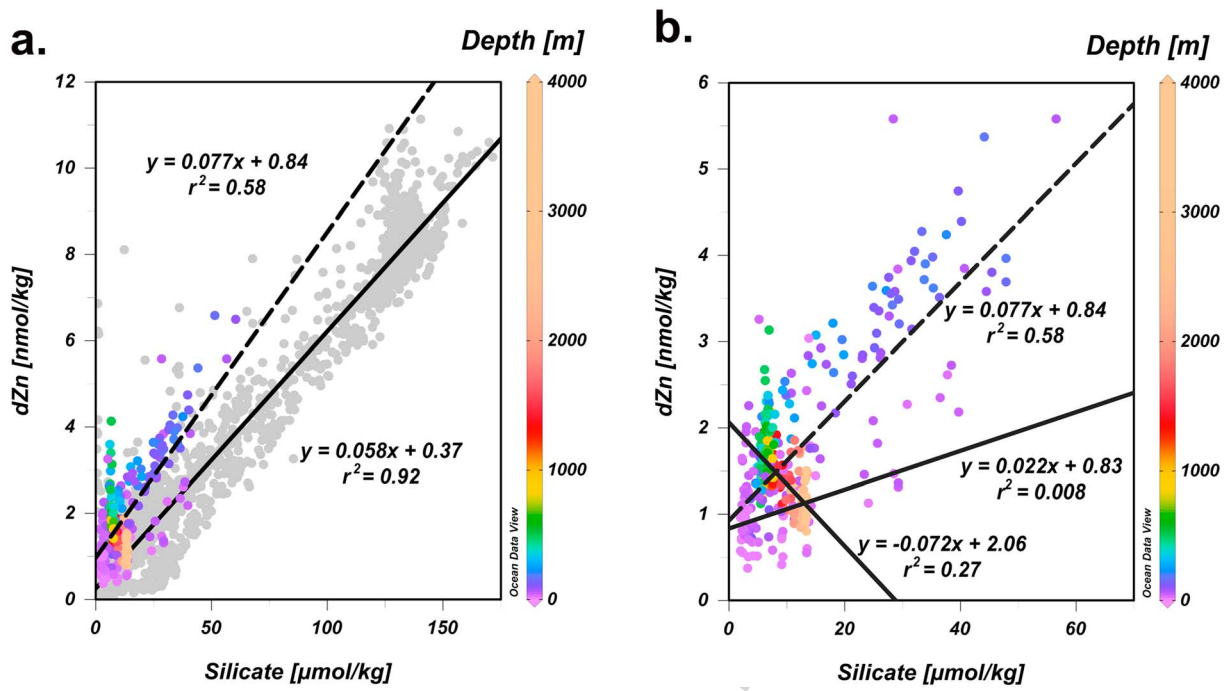

Figure 12. Relationships between dissolved Zn and Si. (a) Zn:Si in the Arctic versus depth (in color), overlaid on top of global Zn:Si from the 2017 GEOTRACES IDP (Schlitzer et al., 2018; in gray). While halocline values fall above the average global Zn:Si slope, intermediate and deep waters fit more closely in the spread of Zn:Si. (b) Zn:Si in the Arctic with depth (in color) showing full water column slope (dotted line), >1,000 m (negative slope), and >2,000 m (positive slope and solid). This demonstrates the decoupling of dissolved zinc (dZn) and Si in Arctic deep waters.

3.5.3. Interbasin Differences

Nutrient-type metal concentrations in deep waters of the global ocean are usually sourced by the remineralization of vertically settling phytoplankton debris. Thus, we attributed the remarkably low and consistent Western Arctic deep water dZn concentrations to a negligible regenerative dZn supply from the low-productivity surface Arctic and, instead, to a simple advective supply of low dZn from the North Atlantic and Eurasian Basins.

However, the Western Arctic's Amerasian Basin is isolated from the Eastern Arctic's Eurasian Basin by the Lomosonov Ridge (1,870-m sill; Rudels, 2015; Timmermans & Garrett, 2006; Timmermans et al., 2003). Above the sill, Arctic dZn concentrations at 1,000- to 1,800-m depth in the Amerasian's Makarov Basin (1.44 ± 0.18 nmol/kg at Stations 30 and 38 closest to the Lomonosov Ridge) were identical to the Eurasian's Amundsen Basin dZn (1.46 ± 0.21 nmol/kg, 1,000–1,800 m, Station 32). This is consistent with active exchange between the basins above the sill and no significant inputs (including remineralization) to or scavenging removal from this layer. Amundsen-Makarov exchange below the ~1,870-m sill is likely intermittent, with the flow direction dependent on the pressure gradient at the sill, which varies over time (Björk et al., 2007; Rudels, 2015). Below 1,800 m, dZn in the two Makarov Basin stations decreased to a low and homogenous 0.97 ± 0.10 nmol/kg compared with the Amundsen Basin dZn of 1.22 ± 0.14 nmol/kg from which they are thought to derive. In contrast to dZn, the Si concentrations increased from the Amundsen to the Makarov stations between 1,000 and 2,000 m (6.7 ± 0.6 to 12.1 ± 0.7 µmol/kg) and again below 2,000 m (12.6 ± 0.9 µmol/kg). Thus, dZn and Si are each homogenous below ~2,000 m but are decoupled (Figure 12, discussed next in section 3.6). F12

The Western Arctic's Makarov and Canada subbasins are separated by the ~2,200-m Alpha and Mendeleev Ridges (Figure 1), which contain a deep gap (~2,400 m) where deep water exchange between the two basins is possible. While the ventilation timescale is perhaps too long to capture significant changes in dZn at these depths, dissolved Si and Al concentrations indicate water flow from the Canada Basin to the Makarov Basin via the Mendeleev Ridge near ~2,500 m (Middag et al., 2009; Swift et al., 1997). During GN01, we observed no significant difference between dZn in deep waters (>2,000 m) of the Canada Basin (1.17 ± 0.30 nmol/kg) compared with the Makarov Basin (1.09 ± 0.20 nmol/kg), despite their ~100-year estimated age difference

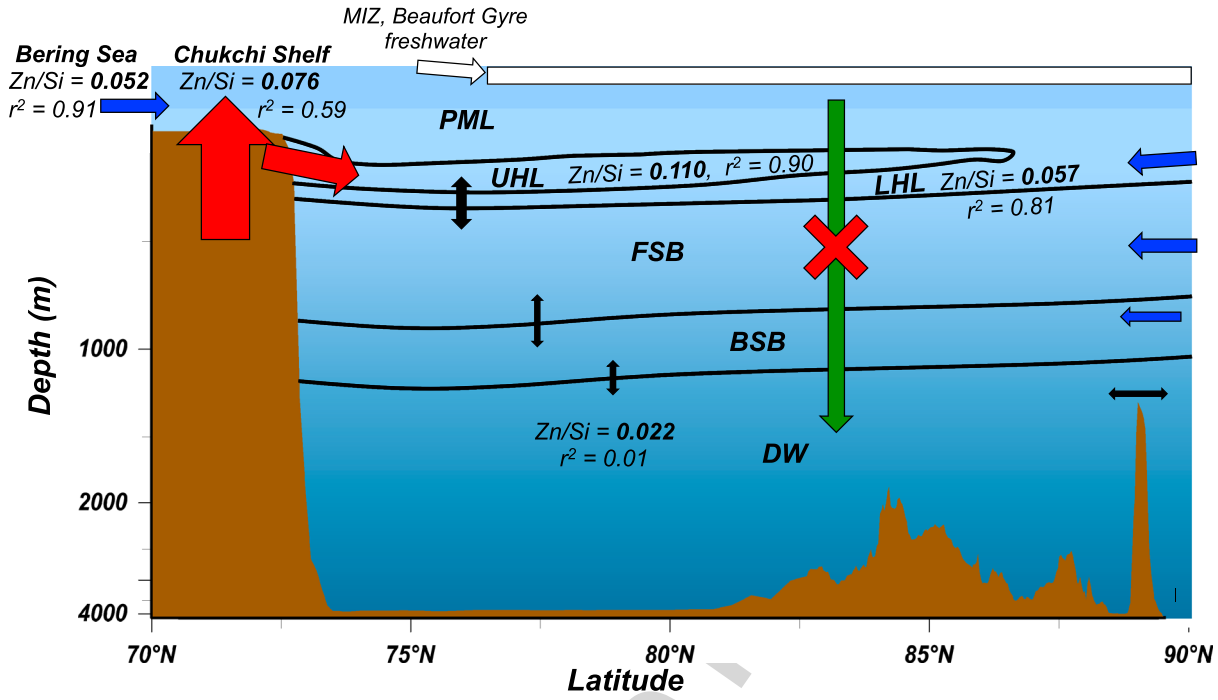

Figure 13. Summary schematic of the major sources of dissolved zinc to the Western Arctic, where relative arrow size reflects the magnitude of the source. (red) Major inputs such as the Chukchi Shelf and halocline. (blue) External water masses such as the Atlantic and Pacific Oceans. (white) Freshwater inputs from the MIZ and riverine sources. (black) The influence of mixing on deep waters below the halocline. (green) Indicates the lack of observed vertical biological regeneration that we would expect to influence deep water dZn distributions. Zn:Si water column regression slopes are also shown for the shelf, halocline, and deep water (>2,000 m), highlighting the evolution of this stoichiometry.

(Tanhua et al., 2009). This is consistent with (1) the hypothesized Canada-Makarov subbasin exchange, (2) a lack of vertically remineralized dZn inputs to depth due to low biological production below the surface sea ice, as above, and (3) a lack of reversible scavenging suggested by Weber et al. (2018).

3.6. Zn:Si Global Comparison

The oceanic relationship between dZn and Si is tied to the biological pump and global thermohaline circulation (Bruland et al., 1978;Vance et al., 2017 ; Weber et al., 2018). However, along GN01, nutrients and nutrient-type metals such as dZn do not exhibit in situ deep water regeneration. Consequently, across the entire GN01 Arctic transect (excluding Pacific Station 1), the Zn:Si slope (0.077 ± 0.004 nmol/μmol, $r^2 = 0.58$) is higher and weaker than the global average (0.060 ± 0.0003 nmol/μmol, $r^2 = 0.95$ [Schlitzer et al., 2018]), the eastern and western North Pacific (0.054 nmol/μmol, $r^2 = 0.99$ and 0.059 nmol/μmol, $r^2 = 0.99$, respectively; Bruland, 1980; Kim et al., 2015), and the central North Atlantic (0.058 nmol/μmol; $r^2 = 0.76$ [Roshan & Wu, 2015]), but it is lower than the oxygenated waters of the HNLC subarctic northeast Pacific (0.102 nmol/μmol, $r^2 = 0.92$ [Janssen & Cullen, 2015]). The high Arctic Zn:Si slope is driven by the higher Zn:Si regression in the shelf bottom waters and in the halocline downstream, but the overall more scattered (lower r^2) Zn:Si relationship is due to Arctic deep waters, where dZn and Si are decoupled (Figures 12a and 13). F13

The North Pacific end member Zn:Si regression at GN01 Station 1 in the Bering Sea (0.052 ± 0.010 nmol/μmol, upper 100 m) is oceanographically consistent with the global average. Along the Bering and Chukchi shelves, this Zn:Si slope increases (0.076 ± 0.012 nmol/μmol, Stations 2–8 and 61–66) due to "soft-tissue" sediment porewater remineralization inputs richer in dZn than in Si (see sections 3.2 and 3.3 above) and becomes even higher within the Canada Basin UHL (0.11 ± 0.01 nmol/μmol), which is formed from the bottommost (brine-rich) waters of the Chukchi shelf. In Arctic intermediate and deep waters, Zn:Si shifts to negative slopes (Figure 12b) because dZn concentrations decrease from 1.76 ± 0.29 nmol/kg between 300 and 500 m to 1.03 ± 0.18 nmol/kg below 3,650 m in Arctic deep water, while Si

concentrations increase from 6.81 ± 0.97 μmol/kg to 12.71 ± 0.84 μmol/kg over the same depths (Figure 3). This decoupling of Zn:Si lies in contrast to our global view of coupled Zn:Si driven by deep water remineralization (Figure 12a, [Bruland et al., 1978; Lohan et al., 2002]). More recent work suggests that Zn:Si ratios are driven by interactions between biogeochemistry and physical processes occurring in the Southern Ocean, leading to water mass mixing of these preformed ratios in addition to scavenging and remineralization (Vance et al., 2017; Weber et al., 2018). We hypothesize three potential causes of this Arctic deep water Zn:Si decoupling: scavenging removal of dZn at depth, a source of Si from deep Artic sediments, or deep water ventilation from waters containing a different Zn:Si ratio.

Pacific Ocean results from Janssen and Cullen (2015) show preferential removal of dZn relative to Si, resulting in low Zn:Si slopes in low-oxygen environments due to hypothesized precipitation of Zn sulfides. However, we see well-oxygenated waters (>200 μmol/kg) throughout deep waters of the Arctic, making Zn sulfide precipitation unlikely. It has been hypothesized that up to 1% of the dZn pool is subject to scavenging (John & Conway, 2014), which could explain the deep Si enrichment compared to dZn, though these studies have focused on upper ocean dZn scavenging onto organic particles, concentrations of which are negligible in Arctic deep waters. In contrast, recent work demonstrates that a reversibly scavenged pool of dZn may account for a significant portion of deep water column dZn (Weber et al., 2018), likely resulting in dZn accumulation with age. However, we observe statistically insignificant differences in deep water dZn between the Canada, Makarov, and Amundsen Basins, despite >100-year age differences between each, which is at odds with any scavenging or addition upon aging. In short, the entire Arctic appears to have homogenously low Zn:Si compared to surface waters, despite century-scale aging of deep waters.

One might also hypothesize that Si fluxes from deep Arctic sediments in a relatively isothermal, isohaline water column could cause an increase in Si without a concomitant release of dZn, given the 1,000-fold lower Zn:Si ratios in diatomaceous frustules compared to water column phytoplankton in this study (Andersen et al., 2011; Ellwood & Hunter, 1999; Hendry & Rickaby, 2008). However, benthic Si fluxes were found to be quite low throughout the Arctic, likely due to low export of biogenic opal (März et al., 2015). If we assume that the long deep water residence times in the Canada and Makarov Basins are due to slow ventilation, we can estimate an accumulation of Si coming from this benthic flux in the deep water, in addition to the preformed Atlantic signature. The total off-shelf area in the Canada and Makarov Basins is 2.1×10^6 km^2 (Jakobsson et al., 2004) with an average depth of 3,400 m based on this transect. Given that the Si maximum extends from 2,000 m to the bottom, we estimate that the total deep water volume is 3.3×10^9 km^3 below 2,000-m depth in the Makarov and Canada Basins. The extrapolated total dSi flux from off-shelf sediments thus ranges from $4.5–68 \times 10^9$ mol/year (März et al., 2015), resulting in 0.40–6.03 μmol/kg of additional or sediment-derived Si supplied to the Canada and Makarov Basin over 300 years (a median estimate of the deep water age in the Makarov and Canada Basins [Tanhua et al., 2009]). The "background" dSi in the Atlantic layer is 6.24 ± 0.60 μmol/kg, while the deep water is 12.58 ± 0.85 μmol/kg, giving an average excess dSi of 6.34 ± 1.04 μmol/kg. Thus, only the upper end of the estimate proffered in März et al. (2015) is nearly equivalent to the average excess of dSi in the deep Western Arctic waters. Thus, only if dSi were sourced from deep Arctic porewaters at the highest measured rates across the entire open Arctic could a sedimentary Si source explain the Zn:Si decoupling, and this all must occur without any porewater dZn inputs; this seems unlikely to be the complete explanation.

We observed negative Zn:Si slopes below 1,000 m (−0.072 ± 0.010 nmol/μmol, $r^2 = 0.27$, Figure 12b), and the Zn:Si relationship fell apart completely below 2,000 m (0.022 ± 0.04 nmol/μmol, $r^2 = 0.008$, Figure 12b). It appears that the Zn:Si slopes in the BSB layer (~1,000–2,000 m) of the Atlantic Water and Zn:Si slopes in the Arctic deep waters are each homogenous but distinct from each other (Figure 12b). This important clue leads us to a water mass explanation. We posit that the homogeneity of the deep layer likely represents deep water renewal from nearly 500 years ago (Timmermans et al., 2003), dating back to the Little Ice Age (Paasche & Bakke, 2010). Lower productivity (Chan et al., 2017), as well as circulation changes driven by the greater ice coverage and lower temperature (Aagaard & Carmack, 1989), could have resulted in different community composition and thus different Zn:Si ratios compared to what we currently observe in the surface and shelves. In a basin marked by low productivity and advective water mass movement, differences in the nutrient stoichiometry in these deepest water layers is unsurprising.

4. Conclusions

Dissolved Zn distributions in the Western Arctic Ocean represent a departure from the classic, "nutrient-type" profile that is prevalent in the global ocean. Rather than being influenced primarily by the biological pump, resulting in low-surface concentrations and regeneration with depth, the Arctic dZn biogeochemistry is governed by a combination of (1) dZn-rich benthic shelf remineralization inputs that are advected into the subsurface western basins and (2) mixing of preformed dZn concentrations from the Atlantic and past ventilation events. Over the shelf, biological processing of dZn is significant, but moving offshore in the surface PML, effects of biological uptake are small, and sea ice melt dilutes dZn in this study, despite previous reports of high dZn concentrations within Arctic sea ice (Tovar-Sánchez et al., 2010). Likewise, no clear riverine source was observed despite elevated dZn concentrations in Arctic rivers (Hölemann et al., 2005). Surface concentrations are primarily determined by incoming Pacific water through the Bering Strait modified by shelf sediment fluxes following the porewater remineralization of high Zn:C and Zn:Si phytoplankton cells.

This high-Zn signature is preserved in the shelf-derived UHL of the Canada Basin, where a maximum in macronutrients and dZn was observed at every station. The dZn-enriched UHL feature dominates the Arctic profile and remains distinctly similar to the shelf in both concentration range and stoichiometry of Zn:Si and Zn:C regression slopes (Figure 13), which compare well with cellular stoichiometries of phytoplankton on the Chukchi Shelf not from open Arctic cells. The Chukchi Shelf seems uniquely suited to provide this signal due to its high seasonal productivity within a shallow water column, leading to efficient export of organic matter to the sediments and allowing brine-rejected waters to contact the sediment surface, from which nutrients are remineralized. This is in contrast to the Canada Basin LHL, which is Eurasian shelf-derived, and exhibits relatively low dZn concentrations that appear to represent a mixture between the overlying UHL and the underlying Atlantic layer. While brine-rejected waters also contact the sediment surface on the Eurasian Shelf, we argue that the lower dZn in Eurasian-derived halocline layers (such as the LHL) occurs because of the deeper Eurasian shelf water column depths, in which more dZn can be remineralized in the water column, preventing the significant porewater remineralization nutrient fluxes observed in the shallower Chukchi Shelf.

The warm Atlantic layer is an easily traceable water mass that serves as an excellent illustration of the effects of mixing on dZn distribution in the Arctic. With potential temperatures >0 °C, this layer originates from the warmer, low-nutrient, low-dZn North Atlantic. As it circulates through the Arctic, it loses heat through conservative mixing with the halocline above. We observe that dZn has a linear relationship with potential temperature in this layer, suggesting that the dZn derives entirely from conservative mixing with the overlying dZn-rich halocline layers. This illustrates how mixing controls intermediate dZn concentrations not in situ remineralization as might be expected for a nutrient-type element.

Overall, in deep waters we find that while dZn fluxes to the Amundsen Basin from hydrothermal sources and to the Makarov Basin from BNL sources may be present, they are small (≤0.3 nmol/kg). With little regenerative inputs to depth, dZn concentrations in Western Arctic deep water are consistently low and are decoupled from the macronutrient Si, likely because of changes in source water stoichiometry over ventilation timescales and/or from low but steady sediment porewater Si fluxes over the long lifetimes of Arctic deep waters.

Acknowledgments
We would like to thank Michael Ellwood and Rob Middag for their thoughtful comments on this paper, the Captain and crew of the USCGC *Healy*; Dave Kadko and Greg Cutter for cruise leadership; Gabi Weiss and Simone Moos for sample collection at sea; Luz Romero for assistance with ICP-MS analyses; Angelica Pasqualini, Bob Newton, Peter Schlosser and Tobias Koffman for contribution of their oxygen isotope measurements and freshwater model estimates; Dan Ohnemus, Liz Mann, and Olga Antipova for assisting with SXRF analyses; Reiner Schlitzer at AWI for use of the Ocean Data View product (https://odv.awi.de), and the SIO ODF team for nutrient, oxygen, and salinity analyses. This work was supported by NSF OCE 1434493 and 1713677 to J. N. F. and R. M. S., B. S. T. and S. R. were supported by NSF OCE 1435862, and N. J. W. and W. M. L. were supported by NSF OCE 1435862. Additionally, this research used resources of the Advanced Photon Source, a U.S. Department of Energy (DOE) Office of Science User Facility operated for the DOE Office of Science by Argonne National Laboratory under Contract DE-AC02-06CH11357. Dissolved zinc, macronutrient, and dissolved oxygen data included in this paper are available under supporting information. Temperature, salinity, and macronutrient data are taken from the Biological and Chemical Oceanography Data Management Office (BCO-DMO) repository (https://www.bco-dmo.org/dataset/647259).

References

Aagaard, K. (1981). On the deep circulation in the Arctic Ocean. *Deep Sea Research Part A Oceanographic Research Papers*, *28*(3), 251–268. https://doi.org/10.1016/0198-0149(81)90066-2

Aagaard, K., & Carmack, E. C. (1989). The role of sea ice and other fresh water in the Arctic circulation. *Journal of Geophysical Research*, *94*(C10), 14,485–14,498. https://doi.org/10.1029/JC094iC10p14485

Aagaard, K., Swift, J. H., & Carmack, E. C. (1985). Thermohaline circulation in the Arctic Mediterranean Seas. *Journal of Geophysical Research*, *90*(C3), 4833–4846. https://doi.org/10.1029/JC090iC03p04833

Aguilar-Islas, A. M., Rember, R., Nishino, S., Kikuchi, T., & Itoh, M. (2013). Partitioning and lateral transport of iron to the Canada Basin. *Polar Science*, *7*(2), 82–99. https://doi.org/10.1016/j.polar.2012.11.001

Andersen, M. B., Vance, D., Archer, C., Anderson, R. F., Ellwood, M. J., & Allen, C. S. (2011). The Zn abundance and isotopic composition of diatom frustules, a proxy for Zn availability in ocean surface seawater. *Earth and Planetary Science Letters*, *301*(1-2), 137–145. https://doi.org/10.1016/j.epsl.2010.10.032

Anderson, L. G., Andersson, P. S., Björk, G., Peter Jones, E., Jutterström, S., & Wåhlström, I. (2013). Source and formation of the upper halocline of the Arctic Ocean. *Journal of Geophysical Research: Oceans*, *118*, 410–421. https://doi.org/10.1029/2012JC008291

Arrigo, K. R., T. Mock, and M. Lizotte (2003), Primary production in sea ice, Sea ice: An introduction to its physics, chemistry, biology and geology, 143–183, DOI: https://doi.org/10.1002/9780470757161.ch5

Björk, G., Jakobsson, M., Rudels, B., Swift, J. H., Anderson, L., Darby, D. A., et al. (2007). Bathymetry and deep-water exchange across the central Lomonosov Ridge at 88–89 N. *Deep Sea Research Part I: Oceanographic Research Papers*, *54*(8), 1197–1208. https://doi.org/10.1016/j.dsr.2007.05.010

Bluhm, B. A., Kosobokova, K. N., & Carmack, E. C. (2015). A tale of two basins: An integrated physical and biological perspective of the deep Arctic Ocean. *Progress in Oceanography*, *139*(Supplement C), 89–121.

Boyd, P. W., Ellwood, M. J., Tagliabue, A., & Twining, B. S. (2017). Biotic and abiotic retention, recycling and remineralization of metals in the ocean. *Nature Geoscience*, *10*(3), 167–173. https://doi.org/10.1038/ngeo2876

Brugler, E. T., Pickart, R. S., Moore, G., Roberts, S., Weingartner, T. J., & Statscewich, H. (2014). Seasonal to interannual variability of the Pacific water boundary current in the Beaufort Sea. *Progress in Oceanography*, *127*, 1–20. https://doi.org/10.1016/j.pocean.2014.05.002

Bruland, K. W. (1980). Oceanographic distributions of cadmium, zinc, nickel, and copper in the North Pacific. *Earth and Planetary Science Letters*, *47*(2), 176–198. https://doi.org/10.1016/0012-821X(80)90035-7

Bruland, K. W. (1989). Complexation of zinc by natural organic ligands in the central North Pacific. *Limnology and Oceanography*, *34*(2), 269–285. https://doi.org/10.4319/lo.1989.34.2.0269

Bruland, K. W., Donat, J. R., & Hutchins, D. A. (1991). Interactive influences of bioactive trace metals on biological production in oceanic waters. *Limnology and Oceanography*, *36*(8), 1555–1577. https://doi.org/10.4319/lo.1991.36.8.1555

Bruland, K. W., Knauer, G. A., & Martin, J. H. (1978). Zinc in north-east Pacific water. *Nature*, *271*(5647), 741–743. https://doi.org/10.1038/271741a0

Bruland, K. W., & Lohan, M. C. (2003). 6.02—Controls of trace metals in seawater. In H. D. H. K. Turekian (Ed.), *Treatise on geochemistry* (pp. 23–47). Pergamon, Oxford. https://doi.org/10.1016/B0-08-043751-6/06105-3 Q12

Cai, M. H., Lin, J., Hong, Q. Q., Wang, Y., & Cai, M. G. (2011). Content and distribution of trace metals in surface sediments from the northern Bering Sea, Chukchi Sea and adjacent Arctic areas. *Marine Pollution Bulletin*, *63*(5-12), 523–527. https://doi.org/10.1016/j.marpolbul.2011.02.007

Carpenter, J. H. (1965). The Chesapeake Bay Institute technique for the Winkler dissolved oxygen method. *Limnology and Oceanography*, *10*(1), 141–143. https://doi.org/10.4319/lo.1965.10.1.0141

Chan, P., Halfar, J., Adey, W., Hetzinger, S., Zack, T., Moore, G. W. K., et al. (2017). Multicentennial record of Labrador Sea primary productivity and sea-ice variability archived in coralline algal barium. *Nature Communications*, *8*, 15,543. https://doi.org/10.1038/ncomms15543

Chang, B. X., & Devol, A. H. (2009). Seasonal and spatial patterns of sedimentary denitrification rates in the Chukchi Sea. *Deep Sea Research Part II: Topical Studies in Oceanography*, *56*(17), 1339–1350. https://doi.org/10.1016/j.dsr2.2008.10.024

Cid, A. P., Nakatsuka, S., & Sohrin, Y. (2012). Stoichiometry among bioactive trace metals in the Chukchi and Beaufort Seas. *Journal of Oceanography*, *68*(6), 985–1001. https://doi.org/10.1007/s10872-012-0150-8

Coachman, L. K., & Barnes, C. A. (1963). The movement of Atlantic Water in the Arctic Ocean. *ARCTIC*, *16*(1 *(1963):* March), 1–80.

Conway, T. M., & John, S. G. (2014). The biogeochemical cycling of zinc and zinc isotopes in the North Atlantic Ocean. *Global Biogeochemical Cycles*, *28*, 1111–1128. https://doi.org/10.1002/2014GB004862

Conway, T. M., & John, S. G. (2015). The cycling of iron, zinc and cadmium in the North East Pacific Ocean—Insights from stable isotopes. *Geochimica et Cosmochimica Acta*, *164*, 262–283. https://doi.org/10.1016/j.gca.2015.05.023

Corlett, W. B., & Pickart, R. S. (2017). The Chukchi slope current. *Progress in Oceanography*, *153*, 50–65. https://doi.org/10.1016/j.pocean.2017.04.005

Cox, A. D., & Saito, M. A. (2013). Proteomic responses of oceanic synechococcus WH8102 to phosphate and zinc scarcity and cadmium additions. *Frontiers in Microbiology*, *4*, 387.

Crawford, D., Lipsen, M., Purdie, D., Lohan, M., Statham, P., Whitney, F., et al. (2003). Influence of zinc and iron enrichments on phytoplankton growth in the northeastern subarctic Pacific. *Limnology and Oceanography*, *48*(4), 1583–1600. https://doi.org/10.4319/lo.2003.48.4.1583

Croot, P. L., Baars, O., & Streu, P. (2011). The distribution of dissolved zinc in the Atlantic sector of the Southern Ocean. *Deep Sea Research Part II: Topical Studies in Oceanography*, *58*(25–26), 2707–2719. https://doi.org/10.1016/j.dsr2.2010.10.041

Culberson, C. H., G. P. Knapp, M. C. Stalcup, R. T. Williams, and F. Zemlyak (1991), A comparison of methods for the determination of dissolved oxygen in seawater.

Cutter, G., Andersson, P., Codispoti, L., Croot, P., Francois, R., Lohan, M., et al. (2010), Sampling and sample-handling protocols for GEOTRACES cruises, edited, GEOTRACES.

Danielsson, L.-G., & Westerlund, S. (1983). Trace metals in the Arctic Ocean. In C. S. Wong, E. Boyle, K. W. Bruland, J. D. Burton, & E. D. Goldberg (Eds.), *Trace metals in sea water* (pp. 85–95). Boston, MA: Springer US. https://doi.org/10.1007/978-1-4757-6864-0_5

Edmonds, H. N., Michael, P. J., Baker, E. T., Connelly, D. P., Snow, J. E., Langmuir, C. H., et al. (2003). Discovery of abundant hydrothermal venting on the ultraslow-spreading Gakkel ridge in the Arctic Ocean. *Nature*, *421*(6920), 252–256. https://doi.org/10.1038/nature01351

Ellwood, M. J. (2008). Wintertime trace metal (Zn, Cu, Ni, Cd, Pb and Co) and nutrient distributions in the subantarctic zone between 40–52 S; 155–160 E. *Marine Chemistry*, *112*(1–2), 107–117. https://doi.org/10.1016/j.marchem.2008.07.008

Ellwood, M. J., and K. Hunter (1999), Determination of the Zn/Si ratio in diatom opal: A method for the separation, cleaning and dissolution of diatoms, 149–160 pp.

Ellwood, M. J., & Hunter, K. A. (2000). The incorporation of zinc and iron into the frustule of the marine diatom Thalassiosira pseudonana. *Limnology and Oceanography*, *45*(7), 1517–1524. https://doi.org/10.4319/lo.2000.45.7.1517

Ellwood, M. J., & van den Berg, C. M. (2000). Zinc speciation in the northeastern Atlantic Ocean. *Marine Chemistry*, *68*(4), 295–306. https://doi.org/10.1016/S0304-4203(99)00085-7

Fitzsimmons, J. N., & Boyle, E. A. (2012). An intercalibration between the GEOTRACES GO-FLO and the MITESS/Vanes sampling systems for dissolved iron concentration analyses (and a closer look at adsorption effects). *Limnology and Oceanography: Methods*, *10*(6), 437–450.

Fitzsimmons, J. N., Carrasco, G. G., Wu, J., Roshan, S., Hatta, M., Measures, C. I., et al. (2015). Partitioning of dissolved iron and iron isotopes into soluble and colloidal phases along the GA03 GEOTRACES North Atlantic transect. *Deep-Sea Research Part II: Topical Studies in Oceanography*, *116*, 130–151. https://doi.org/10.1016/j.dsr2.2014.11.014

Franck, V. M., Bruland, K. W., Hutchins, D. A., & Brzezinski, M. A. (2003). Iron and zinc effects on silicic acid and nitrate uptake kinetics in three high-nutrient, low-chlorophyll (HNLC) regions. *Marine Ecology Progress Series*, *252*, 15–33. https://doi.org/10.3354/meps252015

Gardner, W. D., Richardson, M. J., & Mishonov, A. V. (2018). Global assessment of benthic nepheloid layers and linkage with upper ocean dynamics. *Earth and Planetary Science Letters*, *482*(Supplement C), 126–134.
Gobeil, C., Sundby, B., Macdonald, R., & Smith, J. (2001). Recent change in organic carbon flux to Arctic Ocean deep basins: Evidence from acid volatile sulfide, manganese and rhenium discord in sediments. *Geophysical Research Letters*, *28*(9), 1743–1746. https://doi.org/10.1029/2000GL012491
Gosnell, K. J., Landing, W. M., & Milne, A. (2012). Fluorometric detection of total dissolved zinc in the southern Indian Ocean. *Marine Chemistry*, *132*, 68–76.
Hendry, K. R., & Rickaby, R. E. M. (2008). Opal (Zn/Si) ratios as a nearshore geochemical proxy in coastal Antarctica. *Paleoceanography*, *23*, PA2218. https://doi.org/10.1029/2007PA001576
Hillebrand, H., Dürselen, C. D., Kirschtel, D., Pollingher, U., & Zohary, T. (1999). Biovolume calculation for pelagic and benthic microalgae. *Journal of Phycology*, *35*(2), 403–424. https://doi.org/10.1046/j.1529-8817.1999.3520403.x
Hioki, N., Kuma, K., Morita, Y., Sasayama, R., Ooki, A., Kondo, Y., Obata, H., et al. (2014). Laterally spreading iron, humic-like dissolved organic matter and nutrients in cold, dense subsurface water of the Arctic Ocean. *Scientific Reports*, *4*, 6775.
Hölemann, J. A., Schirmacher, M., & Prange, A. (2005). Seasonal variability of trace metals in the Lena River and the southeastern Laptev Sea: Impact of the spring freshet. *Global and Planetary Change*, *48*(1–3), 112–125. https://doi.org/10.1016/j.gloplacha.2004.12.008
Hydes, D., M. Aoyama, A. Aminot, K. Bakker, S. Becker, S. Coverly, A. Daniel, et al. (2010), Determination of dissolved nutrients (N, P, Si) in seawater with high precision and inter-comparability using gas-segmented continuous flow analysers.
Jaccard, T., Ariztegui, D., & Wilkinson, K. J. (2009). Incorporation of zinc into the frustule of the freshwater diatom Stephanodiscus hantzschii. *Chemical Geology*, *265*(3-4), 381–386. https://doi.org/10.1016/j.chemgeo.2009.04.016
Jakobsson, M., Grantz, A., Kristoffersen, Y., Macnab, R., MacDonald, R., Sakshaug, E., et al. (2004). The Arctic Ocean: Boundary conditions and background information. In *The organic carbon cycle in the Arctic Ocean*, edited (pp. 1–32). Berlin, Heidelberg: Springer.
Jakuba, R. W., Saito, M. A., Moffett, J. W., & Xu, Y. (2012). Dissolved zinc in the subarctic North Pacific and Bering Sea: Its distribution, speciation, and importance to primary producers. *Global Biogeochemical Cycles*, *26*, GB2015. https://doi.org/10.1029/2010GB004004
Janssen, D. J., & Cullen, J. T. (2015). Decoupling of zinc and silicic acid in the subarctic northeast Pacific interior. *Marine Chemistry*, *177*, 124–133. https://doi.org/10.1016/j.marchem.2015.03.014
John, S., and T. M. Conway (2014), A role for scavenging in the marine biogeochemical cycling of zinc and zinc isotopes, 159–167 pp.
Jones, E. P. (2001). Circulation in the Arctic Ocean. *Polar Research*, *20*(2), 139–146. https://doi.org/10.1111/j.1751-8369.2001.tb00049.x
Jones, E. P., & Anderson, L. G. (1986). On the origin of the chemical properties of the Arctic Ocean halocline. *Journal of Geophysical Research*, *91*(C9), 10,759–10,767. https://doi.org/10.1029/JC091iC09p10759
Jones, E. P., Anderson, L. G., & Swift, J. H. (1998). Distribution of Atlantic and Pacific waters in the upper Arctic Ocean: Implications for circulation. *Geophysical Research Letters*, *25*(6), 765–768. https://doi.org/10.1029/98GL00464
Kadko, D., Galfond, B., Landing, W. M., & Shelley, R. U. (2016). Determining the pathways, fate, and flux of atmospherically derived trace elements in the Arctic ocean/ice system. *Marine Chemistry*, *182*(Supplement C), 38–50.
Kim, T., Obata, H., Kondo, Y., Ogawa, H., & Gamo, T. (2015). Distribution and speciation of dissolved zinc in the western North Pacific and its adjacent seas. *Marine Chemistry*, *173*, 330–341. https://doi.org/10.1016/j.marchem.2014.10.016
Kim, T., Obata, H., Nishioka, J., & Gamo, T. (2017). Distribution of dissolved zinc in the western and central subarctic North Pacific. *Global Biogeochemical Cycles*, *31*, 1454–1468. https://doi.org/10.1002/2017GB005711
Klunder, M. B., Laan, P., Middag, R., de Baar, H. J. W., & Bakker, K. (2012). Dissolved iron in the Arctic Ocean: Important role of hydrothermal sources, shelf input and scavenging removal. *Journal of Geophysical Research*, *117*, C04014. https://doi.org/10.1029/2011JC007135
Kondo, Y., Obata, H., Hioki, N., Ooki, A., Nishino, S., Kikuchi, T., & Kuma, K. (2016). Transport of trace metals (Mn, Fe, Ni, Zn and Cd) in the western Arctic Ocean (Chukchi Sea and Canada Basin) in late summer 2012. *Deep Sea Research Part I: Oceanographic Research Papers*, *116*, 236–252. https://doi.org/10.1016/j.dsr.2016.08.010
Lagerström, M. E., Field, M. P., Séguret, M., Fischer, L., Hann, S., & Sherrell, R. M. (2013). Automated on-line flow-injection ICP-MS determination of trace metals (Mn, Fe, Co, Ni, Cu and Zn) in open ocean seawater: Application to the GEOTRACES program. *Marine Chemistry*, *155*(0), 71–80. https://doi.org/10.1016/j.marchem.2013.06.001
Li, Q., Chen, M., Jia, R., Zeng, J., Lin, H., Zheng, M., & Qiu, Y. (2017). Transit time of river water in the Bering and Chukchi Seas estimated from δ18O and radium isotopes. *Progress in Oceanography*, *159*(Supplement C), 115–129.
Little, S. H., Vance, D., McManus, J., & Severmann, S. (2016). Key role of continental margin sediments in the oceanic mass balance of Zn and Zn isotopes. *Geology*, *44*(3), 207–210. https://doi.org/10.1130/G37493.1
Little, S. H., Vance, D., Walker-Brown, C., & Landing, W. (2014). The oceanic mass balance of copper and zinc isotopes, investigated by analysis of their inputs, and outputs to ferromanganese oxide sediments. *Geochimica et Cosmochimica Acta*, *125*, 673–693. https://doi.org/10.1016/j.gca.2013.07.046
Lohan, M. C., Statham, P. J., & Crawford, D. W. (2002). Total dissolved zinc in the upper water column of the subarctic north East Pacific. *Deep Sea Research Part II: Topical Studies in Oceanography*, *49*(24-25), 5793–5808. https://doi.org/10.1016/S0967-0645(02)00215-1
Macdonald, R. W., Carmack, E., McLaughlin, F., Falkner, K., & Swift, J. (1999). Connections among ice, runoff and atmospheric forcing in the Beaufort Gyre. *Geophysical Research Letters*, *26*(15), 2223–2226. https://doi.org/10.1029/1999GL900508
Macdonald, R. W., Carmack, E. C., McLaughlin, F. A., Iseki, K., Macdonald, D. M., & O'Brien, M. C. (1989). Composition and modification of water masses in the Mackenzie shelf estuary. *Journal of Geophysical Research*, *94*(C12), 18,057–18,070. https://doi.org/10.1029/JC094iC12p18057
Macdonald, R. W., Kuzyk, Z. A., & Johannessen, S. C. (2015). It is not just about the ice: A geochemical perspective on the changing Arctic Ocean. *Journal of Environmental Studies and Sciences*, *5*(3), 288–301. https://doi.org/10.1007/s13412-015-0302-4
Mahaffey, C., Reynolds, S., Davis, C. E., & Lohan, M. C. (2014). Alkaline phosphatase activity in the subtropical ocean: Insights from nutrient, dust and trace metal addition experiments. *Frontiers in Marine Science*, *1*, 73.
Markus, T., Stroeve, J. C., & Miller, J. (2009). Recent changes in Arctic Sea ice melt onset, freezeup, and melt season length. *Journal of Geophysical Research*, *114*, C12024. https://doi.org/10.1029/2009JC005436
Marsay, C. M., Aguilar-Islas, A., Fitzsimmons, J. N., Hatta, M., Jensen, L. T., John, S. G., et al. (2018). Dissolved and particulate trace elements in late summer Arctic melt ponds. *Marine Chemistry*, *204*, 70–85. https://doi.org/10.1016/j.marchem.2018.06.002
März, C., Meinhardt, A.-K., Schnetger, B., & Brumsack, H.-J. (2015). Silica diagenesis and benthic fluxes in the Arctic Ocean. *Marine Chemistry*, *171*, 1–9. https://doi.org/10.1016/j.marchem.2015.02.003
Mawji, E., Schlitzer, R., & Dodas, E. (2015). The GEOTRACES Intermediate Data Product 2014. *Marine Chemistry*, *177*, 1–8. https://doi.org/10.1016/j.marchem.2015.04.005

Menden-Deuer, S., & Lessard, E. J. (2000). Carbon to volume relationships for dinoflagellates, diatoms, and other protist plankton. *Limnology and Oceanography*, *45*(3), 569–579. https://doi.org/10.4319/lo.2000.45.3.0569

Middag, R., de Baar, H., Laan, P., & Bakker, K. (2009). Dissolved aluminium and the silicon cycle in the Arctic Ocean. *Marine Chemistry*, *115*(3-4), 176–195. https://doi.org/10.1016/j.marchem.2009.08.002

Middag, R., de Baar, H. J. W., Laan, P., & Klunder, M. B. (2011). Fluvial and hydrothermal input of manganese into the Arctic Ocean. *Geochimica et Cosmochimica Acta*, *75*(9), 2393–2408. https://doi.org/10.1016/j.gca.2011.02.011

Middag, R., Séférian, R., Conway, T. M., John, S. G., Bruland, K. W., & de Baar, H. J. W. (2015). Intercomparison of dissolved trace elements at the Bermuda Atlantic time series station. *Marine Chemistry*, *177*, 476–489. https://doi.org/10.1016/j.marchem.2015.06.014

Moore, R. M. (1981). Oceanographic distributions of zinc, cadmium, copper and aluminium in waters of the central Arctic. *Geochimica et Cosmochimica Acta*, *45*(12), 2475–2482. https://doi.org/10.1016/0016-7037(81)90099-5

Morel, F. M. M. (2008). The co-evolution of phytoplankton and trace element cycles in the oceans. *Geobiology*, *6*(3), 318–324. https://doi.org/10.1111/j.1472-4669.2008.00144.x

Newton, R., Schlosser, P., Mortlock, R., Swift, J., & MacDonald, R. (2013). Canadian Basin freshwater sources and changes: Results from the 2005 Arctic Ocean section. *Journal of Geophysical Research: Oceans*, *118*, 2133–2154. https://doi.org/10.1002/jgrc.20101

Nishino, S., Shimada, K., & Itoh, M. (2005). Use of ammonium and other nitrogen tracers to investigate the spreading of shelf waters in the western Arctic halocline. *Journal of Geophysical Research*, *110*, C10005. https://doi.org/10.1029/2003JC002118

Noble, A. E., Ohnemus, D. C., Hawco, N. J., Lam, P. J., & Saito, M. A. (2017). Coastal sources, sinks and strong organic complexation of dissolved cobalt within the US North Atlantic GEOTRACES transect GA03. *Biogeosciences*, *14*(11), 2715–2739. https://doi.org/10.5194/bg-14-2715-2017

Nowicki, J. L., Johnson, K. S., Coale, K. H., Elrod, V. A., & Lieberman, S. H. (1994). Determination of zinc in seawater using flow injection analysis with fluorometric detection. *Analytical Chemistry*, *66*(17), 2732–2738. https://doi.org/10.1021/ac00089a021

Núnez-Milland, D. R., Baines, S. B., Vogt, S., & Twining, B. S. (2010). Quantification of phosphorus in single cells using synchrotron X-ray fluorescence. *Journal of Synchrotron Radiation*, *17*(4), 560–566. https://doi.org/10.1107/S0909049510014020

Ohnemus, D. C., & Lam, P. J. (2015). Cycling of lithogenic marine particles in the US GEOTRACES North Atlantic transect. *Deep Sea Research Part II: Topical Studies in Oceanography*, *116*, 283–302. https://doi.org/10.1016/j.dsr2.2014.11.019

Overland, J. E., & Wang, M. (2005). The Arctic climate paradox: The recent decrease of the Arctic Oscillation. *Geophysical Research Letters*, *32*, L06701. https://doi.org/10.1029/2004GL021752

Paasche, Ø., & Bakke, J. (2010). Defining the Little Ice Age. *Climate of the Past Discussions*, *6*(5), 2159–2175. https://doi.org/10.5194/cpd-6-2159-2010

Peterson, B. J., Holmes, R. M., McClelland, J. W., Vörösmarty, C. J., Lammers, R. B., Shiklomanov, A. I., et al. (2002). Increasing river discharge to the Arctic Ocean. *Science*, *298*(5601), 2171–2173. https://doi.org/10.1126/science.1077445

Pickart, R. S., Weingartner, T. J., Pratt, L. J., Zimmermann, S., & Torres, D. J. (2005). Flow of winter-transformed Pacific water into the Western Arctic. *Deep Sea Research Part II: Topical Studies in Oceanography*, *52*(24-26), 3175–3198. https://doi.org/10.1016/j.dsr2.2005.10.009

Proshutinsky, A., Bourke, R. H., & McLaughlin, F. A. (2002). The role of the Beaufort Gyre in Arctic climate variability: Seasonal to decadal climate scales. *Geophysical Research Letters*, *29*(23), 2100. https://doi.org/10.1029/2002GL015847

Roshan, S., & Wu, J. (2015). Water mass mixing: The dominant control on the zinc distribution in the North Atlantic Ocean. *Global Biogeochemical Cycles*, *29*, 1060–1074. https://doi.org/10.1002/2014GB005026

Roshan, S., Wu, J., & Jenkins, W. J. (2016). Long-range transport of hydrothermal dissolved Zn in the tropical South Pacific. *Marine Chemistry*, *183*, 25–32. https://doi.org/10.1016/j.marchem.2016.05.005

Rudels, B. (2015). Arctic Ocean circulation, processes and water masses: A description of observations and ideas with focus on the period prior to the International Polar Year 2007–2009. *Progress in Oceanography*, *132*, 22–67. https://doi.org/10.1016/j.pocean.2013.11.006

Rudels, B., Jones, E. P., Anderson, L. G., & Kattner, G. (1994). On the intermediate depth waters of the Arctic Ocean. In *The polar oceans and their role in shaping the global environment*, edited (pp. 33–46). American Geophysical Union.

Rudels, B., Jones, E. P., Schauer, U., & Eriksson, P. (2004). Atlantic sources of the Arctic Ocean surface and halocline waters. *Polar Research*, *23*(2), 181–208. https://doi.org/10.1111/j.1751-8369.2004.tb00007.x

Rutgers van der Loeff, M., Cai, P., Stimac, I., Bauch, D., Hanfland, C., Roeske, T., & Moran, S. B. (2012). Shelf-basin exchange times of Arctic surface waters estimated from 228Th/228Ra disequilibrium. *Journal of Geophysical Research*, *117*, C03024. https://doi.org/10.1029/2011JC007478

Rutgers van der Loeff, M., Meyer, R., Rudels, B., & Rachor, E. (2002). Resuspension and particle transport in the benthic nepheloid layer in and near Fram Strait in relation to faunal abundances and 234Th depletion. *Deep Sea Research Part I: Oceanographic Research Papers*, *49*(11), 1941–1958. https://doi.org/10.1016/S0967-0637(02)00113-9

Sakshaug, E. (2004). *Primary and secondary production in the Arctic Seas, in The organic carbon cycle in the Arctic Ocean*, edited, (pp. 57–81). Berlin, Heidelberg: Springer.

Schauer, U., Rudels, B., Jones, E., Anderson, L., Muench, R., Björk, G., et al. (2002), Confluence and redistribution of Atlantic water in the Nansen, Amundsen and Makarov basins, paper presented at Annales Geophysicae.

Schlitzer, R. (2016), Ocean data view, http://odv. *awi. de*.

Schlitzer, R., Anderson, R. F., Dodas, E. M., Lohan, M., Geibert, W., Tagliabue, A., et al. (2018). The GEOTRACES Intermediate Data Product 2017. *Chemical Geology*, *493*, 210–223. https://doi.org/10.1016/j.chemgeo.2018.05.040

Schlosser, P., Kromer, B., Ekwurzel, B., Bönisch, G., McNichol, A., Schneider, R., et al. (1997). The first trans-Arctic 14C section: Comparison of the mean ages of the deep waters in the Eurasian and Canadian basins of the Arctic Ocean. *Nuclear Instruments and Methods in Physics Research Section B: Beam Interactions with Materials and Atoms*, *123*(1–4), 431–437. https://doi.org/10.1016/S0168-583X(96)00677-5

Shaked, Y., Xu, Y., Leblanc, K., & Morel, F. M. (2006). Zinc availability and alkaline phosphatase activity in Emiliania huxleyi: Implications for Zn-P co-limitation in the ocean. *Limnology and Oceanography*, *51*(1), 299–309. https://doi.org/10.4319/lo.2006.51.1.0299

Shimada, K., Itoh, M., Nishino, S., McLaughlin, F., Carmack, E., & Proshutinsky, A. (2005). Halocline structure in the Canada Basin of the Arctic Ocean. *Geophysical Research Letters*, *32*, L03605. https://doi.org/10.1029/2004GL021358

Sohrin, Y., Urushihara, S., Nakatsuka, S., Kono, T., Higo, E., Minami, T., Norisuye, K., et al. (2008). Multielemental determination of GEOTRACES key trace metals in seawater by ICPMS after Preconcentration using an ethylenediaminetriacetic acid chelating resin. *Analytical Chemistry*, *80*(16), 6267–6273. https://doi.org/10.1021/ac800500f

Sunda, W. G., & Huntsman, S. A. (1995). Cobalt and zinc interreplacement in marine phytoplankton: Biological and geochemical implications. *Limnology and Oceanography*, *40*(8), 1404–1417. https://doi.org/10.4319/lo.1995.40.8.1404

Swift, J., Jones, E., Aagaard, K., Carmack, E., Hingston, M., Macdonald, R., et al. (1997). Waters of the Makarov and Canada basins. *Deep Sea Research Part II: Topical Studies in Oceanography*, *44*(8), 1503–1529. https://doi.org/10.1016/S0967-0645(97)00055-6

Tanhua, T., Jones, E. P., Jeansson, E., Jutterström, S., Smethie, W. M., Wallace, D. W. R., & Anderson, L. G. (2009). Ventilation of the Arctic Ocean: Mean ages and inventories of anthropogenic CO2 and CFC-11. *Journal of Geophysical Research*, *114*, C01002. https://doi.org/10.1029/2008JC004868

Timmermans, M.-L., & Garrett, C. (2006). Evolution of the deep water in the Canadian Basin in the Arctic Ocean. *Journal of Physical Oceanography*, *36*(5), 866–874. https://doi.org/10.1175/JPO2906.1

Timmermans, M.-L., Garrett, C., & Carmack, E. (2003). The thermohaline structure and evolution of the deep waters in the Canada Basin, Arctic Ocean. *Deep Sea Research Part I: Oceanographic Research Papers*, *50*(10-11), 1305–1321. https://doi.org/10.1016/S0967-0637(03)00125-0

Timofeyev, V. T. (1962). The movement of Atlantic water and heat into the arctic basin. *Deep Sea Research and Oceanographic Abstracts*, *9*(7-10), 358–361. https://doi.org/10.1016/0011-7471(62)90016-5

Tovar-Sánchez, A., Duarte, C. M., Alonso, J. C., Lacorte, S., Tauler, R., & Galbán-Malagón, C. (2010). Impacts of metals and nutrients released from melting multiyear Arctic sea ice. *Journal of Geophysical Research*, *115*, C07003. https://doi.org/10.1029/2009JC005685

Trefry, J. H., Trocine, R. P., Cooper, L. W., & Dunton, K. H. (2014). Trace metals and organic carbon in sediments of the northeastern Chukchi Sea. *Deep Sea Research Part II: Topical Studies in Oceanography*, *102*, 18–31. https://doi.org/10.1016/j.dsr2.2013.07.018

Twining, B. S. (2018), Contrasts in trace element content of marine phytoplankton from different ocean basins, in *Ocean Sciences Meeting*, Edited, Portland, OR. https://agu.confex.com/agu/os18/preliminaryview.cgi/Session28118

Twining, B. S., & Baines, S. B. (2013). The trace metal composition of marine phytoplankton. *Annual Review of Marine Science*, *5*(1), 191–215. https://doi.org/10.1146/annurev-marine-121211-172322

Twining, B. S., Baines, S. B., Bozard, J. B., Vogt, S., Walker, E. A., & Nelson, D. M. (2011). Metal quotas of plankton in the equatorial Pacific Ocean. *Deep Sea Research Part II: Topical Studies in Oceanography*, *58*(3–4), 325–341. https://doi.org/10.1016/j.dsr2.2010.08.018

Twining, B. S., Baines, S. B., & Fisher, N. S. (2004). Element stoichiometries of individual plankton cells collected during the Southern Ocean Iron Experiment (SOFeX). *Limnology and Oceanography*, *49*(6), 2115–2128. https://doi.org/10.4319/lo.2004.49.6.2115

Twining, B. S., Baines, S. B., Fisher, N. S., Maser, J., Vogt, S., Jacobsen, C., et al. (2003). Quantifying trace elements in individual aquatic protist cells with a synchrotron X-ray fluorescence microprobe. *Analytical Chemistry*, *75*(15), 3806–3816. https://doi.org/10.1021/ac034227z

Twining, B. S., Nodder, S. D., King, A. L., Hutchins, D. A., LeCleir, G. R., DeBruyn, J. M., et al. (2014). Differential remineralization of major and trace elements in sinking diatoms. *Limnology and Oceanography*, *59*(3), 689–704. https://doi.org/10.4319/lo.2014.59.3.0689

Twining, B. S., Rauschenberg, S., Morton, P. L., & Vogt, S. (2015). Metal contents of phytoplankton and labile particulate material in the North Atlantic Ocean. *Progress in Oceanography*, *137*(Part A), 261–283.

Vance, D., Little, S. H., de Souza, G. F., Khatiwala, S., Lohan, M. C., & Middag, R. (2017). Silicon and zinc biogeochemical cycles coupled through the Southern Ocean. *Nature Geoscience*, *10*(3), 202–206. https://doi.org/10.1038/ngeo2890

Weber, T., John, S., Tagliabue, A., & DeVries, T. (2018). Biological uptake and reversible scavenging of zinc in the global ocean. *Science*, *361*(6397), 72–76. https://doi.org/10.1126/science.aap8532

Woodgate, R. A. (2018). Increases in the Pacific inflow to the Arctic from 1990 to 2015, and insights into seasonal trends and driving mechanisms from year-round Bering Strait mooring data. *Progress in Oceanography*, *160*, 124–154. https://doi.org/10.1016/j.pocean.2017.12.007

Woodgate, R. A., Aagaard, K., Muench, R. D., Gunn, J., Björk, G., Rudels, B., et al. (2001). The Arctic Ocean boundary current along the Eurasian slope and the adjacent Lomonosov Ridge: Water mass properties, transports and transformations from moored instruments. *Deep Sea Research Part I: Oceanographic Research Papers*, *48*(8), 1757–1792. https://doi.org/10.1016/S0967-0637(00)00091-1

Woodgate, R. A., Aagaard, K., Swift, J. H., Falkner, K. K., & Smethie, W. M. (2005). Pacific ventilation of the Arctic Ocean's lower halocline by upwelling and diapycnal mixing over the continental margin. *Geophysical Research Letters*, *32*, , L18609. https://doi.org/10.1029/2005GL023999

Wyatt, N. J., Milne, A., Woodward, E. M. S., Rees, A. P., Browning, T. J., Bouman, H. A., et al. (2014). Biogeochemical cycling of dissolved zinc along the GEOTRACES South Atlantic transect GA10 at 40°S. *Global Biogeochemical Cycles*, *28*, 44–56. https://doi.org/10.1002/2013GB004637

Yeats, P. A. (1988). Manganese, nickel, zinc and cadmium distributions at the Fram-3 and Cesar Ice Camps in the Arctic Ocean. *Oceanologica Acta*, *11*(4), 383–388.

Yeats, P. A., & Westerlund, S. (1991). Trace metal distributions at an Arctic Ocean ice island. *Marine Chemistry*, *33*(3), 261–277. https://doi.org/10.1016/0304-4203(91)90071-4

Zhao, Y., Vance, D., Abouchami, W., & de Baar, H. J. (2014). Biogeochemical cycling of zinc and its isotopes in the Southern Ocean. *Geochimica et Cosmochimica Acta*, *125*, 653–672. https://doi.org/10.1016/j.gca.2013.07.045